Large-N reduction in QCD with two adjoint Dirac fermions

Barak Bringoltz, Mateusz Koren, and Stephen R. Sharpe

Phys. Rev. D **85**, 094504 — Published 3 May 2012

DOI: 10.1103/PhysRevD.85.094504

Large-N reduction in QCD with two adjoint Dirac fermions

Barak Bringoltz,[1,2] Mateusz Koren,[3,2] and Stephen R. Sharpe[2]

[1] *IIAR – the Israeli Institute for Advanced Research, Rehovot, Israel*
[2] *Department of Physics, University of Washington, Seattle, WA 98195-1560, USA*
[3] *M. Smoluchowski Institute of Physics, Jagiellonian University, Reymonta 4, 30-059 Cracow, Poland*

(Dated: April 6, 2012)

We use lattice simulations to study the single-site version of $SU(N)$ lattice gauge theory with two flavors of Wilson-Dirac fermions in the adjoint representation, a theory whose large volume correspondent is expected to be conformal or nearly conformal. Working with N as large as 53, we map out the phase diagram in the plane of bare 't Hooft coupling, g^2N, and of the lattice quark mass, am, and look for the region where the Z_N^4 center symmetry of the theory is intact. In this region one expects the large-N equivalence of the single site and infinite volume theories to be valid. As for the $N_f = 1$ case (see Phys. Rev. D **80**: 065031), we find that the center-symmetric region is large and includes both light fermion masses and masses at the cutoff scale. We study the N-dependence of the width of this region and find strong evidence that it remains of finite width as $N \to \infty$. Simulating with couplings as small as $g^2N = 0.005$, we find that the width shrinks slowly with decreasing g^2N, at a rate consistent with analytic arguments. Within the center-symmetric region our results for the phase structure, when extrapolated to $N = \infty$, apply also for the large volume theory, which is minimal walking technicolor at $N = \infty$. We find a first-order transition as a function of am for all values of b, which we argue favors that the theory is confining in the infrared. Finally, we measure the eigenvalue densities of the Wilson-Dirac operator and its hermitian version, and use large Wilson loops to study the utility of reduction for extracting physical observables.

I. INTRODUCTION

There has been a recent revival of interest in the possibility of using complete volume reduction for the infinite N (number of colors) limit of QCD and QCD-like theories. If this reduction holds, then the theory, defined nonperturbatively on a lattice, gives predictions that, at infinite N, are independent of the number of sites. Specifically this means that the theory defined on a single site, or a small, fixed number of sites, is large-N equivalent to the corresponding infinite volume theory with the same bare parameters [1].

Reduction to a single-site has long been known to fail for the pure gauge theory (and thus also for QCD in 't Hooft's large-N limit, since quark contributions are suppressed by $1/N$ in this limit) [2–4]. This failure is due to the breakdown of one of the conditions needed for a large-N orbifold equivalence between the single-site and large volume theories (see Refs. [5] and [6]). This key condition is that the Z_N^4 center symmetry of the single-site theory must be unbroken. This symmetry breaks spontaneously[1] in the single-site pure gauge theory (the Eguchi-Kawai [EK] model [1]). This is expected from perturbation theory (PT), where, at leading order, the effective potential for eigenvalues of the holonomy around the compact direction (the Polyakov loop) leads to attraction and thus clumping [2, 3]. Several years ago, it was realized that the addition of massless fermions that reside in the adjoint representation and that have periodic boundary conditions in the compact directions leads (in perturbation theory) to a repulsion between eigenvalues, which in turn leads to a uniform distribution of these eigenvalues [7]. In this case the center symmetry is unbroken and reduction holds.

Two of us have previously investigated the single-site theory with a single Dirac adjoint fermion (discretized using Wilson fermions), finding that, for small to rather large values of the inverse 't Hooft coupling, $b = 1/(g^2 N) \in [0, 1]$, there is a large range of values of the quark mass for which the center symmetry appears to be unbroken [8]. This result was unanticipated because several leading-order perturbative calculations, done with a single compact direction (or a single site along only one Euclidean direction) show that the symmetry breaks if the physical mass m exceeds a value of $O(1/aN)$ [9–11]. As m increases from $\sim 1/aN$ to $\sim 1/a$, the perturbative calculations indicate that the eigenvalue density of the link in the short direction will form a number of clumps, starting with $O(N)$ clumps at very small masses, and decreasing to a single clump at infinite mass. The results of Ref. [8] (which used N up to 15) do not follow this pattern, instead finding no clumping for masses up to of $O(1/a)$ for all values of N. A semi-quantitative understanding of these results has recently been given in Refs. [11, 12]. With more than two compact dimensions, the fluctuations in the eigenvalues can overwhelm the tendency to clump, and this happens up to masses of $O(1/a)$. The numerical results for the phase diagram obtained in Ref. [8] have also been checked, and extended, in Ref. [11]. We also note that simulations with $N_f = 1/2$, 1 and 2 massless overlap adjoint fermions also find no center-symmetry breaking, at least at large b [13, 14].

In the present paper we extend our investigations to $N_f = 2$. The main motivation for doing so is that the corresponding infinite volume theory is expected to be nearly conformal, and thus a candidate "walking technicolor" model.[2] Indeed the theory with two colors is the theory with the smallest field content that lies close to the conformal window, and has been dubbed the "minimal walking technicolor" (MWT) model. If reduction holds, then we should be able to study a close relative of MWT, i.e. the theory with $N = \infty$. One naively expects only a weak dependence on N, because the number of both gluonic and fermionic degrees of freedom scale as N^2.

We also note that the $N_f = 2$ AEK (Adjoint Eguchi-Kawai) model is related by a combination of orbifold and orientifold equivalences to the QCD-like theory with $2N_f = 4$ fermions in the two index anti-symmetric (AS) irrep [7, 17].[3] This theory in turn is the large-N limit of QCD with $2N_f$ quarks, but with the limit taken with the quarks in the AS irrep (which is equivalent to the anti-fundamental for $N = 3$). This is the Corrigan-Ramond large-N limit of QCD [18], which differs from the 't Hooft limit in having fermion loops.[4]

Our main effort herein is to determine the phase structure of the $N_f = 2$ AEK model. To do so we have upgraded our simulation algorithm from a Metropolis algorithm, with CPU scaling as N^{6-8}, to a Hybrid

[1] Strictly speaking, the symmetry is spontaneously broken only for $N \to \infty$. In practice, however, effective spontaneous symmetry breaking is seen in simulations at finite but large values of N, and we use the terminology of phase transitions throughout this article.

[2] For recent reviews of technicolor models on the lattice, see Refs. [15] and [16].

[3] This equivalence holds only in charge-conjugation even subsectors.

[4] Note that here taking the Corrigan-Ramond limit moves one from a theory which is not close to the conformal window (4 quarks in the fundamental irrep) to one that is (4 quarks in the AS irrep), suggesting that $1/N$ corrections are probably large, at least in this respect.

Monte-Carlo (HMC) algorithm, for which we find CPU $\propto N^{4-4.5}$. This allows us to reach much larger values of N, and to improve the statistics. Together, these advances allow us to study the nature of the symmetry breaking in more detail than in the $N_f = 1$ study [8], allowing us to compare with the theoretical expectations of Refs. [11, 12]. Our main result is that we find the phase diagram to be qualitatively similar to that for $N_f = 1$, with center symmetry remaining unbroken for masses up to $O(1/a)$. Specifically, our evidence suggests that, at fixed coupling, although the range of masses for which the symmetry is unbroken shrinks somewhat as N increases, it remains of width $\sim 1/a$ as $N \to \infty$. Our strongest evidence for this is at $b = 1$, but our results suggest that this holds for $b = 0 - 200$, i.e. for the entire range of coupling that one could possibly be interested in. Thus our results suggest that one can use adjoint fermions of almost any mass to "stabilize" reduction. This is only expected to fail in the extreme weak coupling limit ($b \to \infty$).

This is an encouraging result, and so we have made the first steps in trying to see if reduction can be used to obtain results for physical quantities. The key question is how large a value of N is needed so that the physical contributions are larger than those from $1/N$ effects. We have investigated this by studying the large N extrapolation of the plaquette, by calculating the spectrum of the Wilson-Dirac operator and its hermitian counterpart, and by calculating large Wilson loops in order to see if we can extract the heavy-quark potential.

Work along similar lines has recently been reported in Ref. [19]. These authors simulate the theory with two adjoint Wilson fermions on a 2^4 lattice, and use $N = 2 - 6$. They report evidence that, for $b = 2$, there is a region of quark masses around the putative critical value, including quarks of masses $\sim 1/a$, for which the center symmetry is unbroken.

This paper is organized as follows. In the following section we describe the AEK model and the properties of the large-volume theory to which it would be equivalent were reduction to hold. In Sec. III we describe the algorithm that we use, and show some results concerning its performance. Section IV is the core of the paper, in which we use our numerical results to determine the phase diagram of the AEK model. We then, in Sec. V, present first results for "observables"—the spectra of the Wilson-Dirac operator and its hermitian counterpart, and large Wilson loops. We close in Sec. VI with a summary and a discussion of the outlook for future work. An appendix describes models for eigenvalues of the Wilson-Dirac operator that are used in Sec. V.

II. THE AEK MODEL AND ITS PUTATIVE LARGE-VOLUME EQUIVALENT

The partition function of the single-site theory is

$$Z_{\rm AEK} = \int \prod_{\mu} DU_\mu D\psi D\bar{\psi} \, \exp\left(S_{\rm gauge} + \sum_{j=1}^{N_f} \bar{\psi}_j \, D_{\rm W} \, \psi_j \right), \tag{2.1}$$

where the four U_μ are SU(N) matrices, while $\bar{\psi}_j$ and ψ_j are Grassmann Dirac variables of flavor j, living in the adjoint representation of $SU(N)$. We use the Wilson gauge action

$$S_{\rm gauge} = 2N\, b \sum_{\mu<\nu} {\rm ReTr}\, U_{\mu\nu}^{\rm plaq}\,, \tag{2.2}$$

where $U_{\mu\nu}^{\rm plaq}$ is the product of links around the plaquette in the μ, ν plane, and b is the inverse 't Hooft coupling,

$$b \equiv \frac{1}{g^2 N}\,. \tag{2.3}$$

We also use Wilson's lattice Dirac operator

$$D_W = 1 - \kappa \left[\sum_{\mu=1}^{4} (1-\gamma_\mu)\, U_\mu^{\rm adj} + (1+\gamma_\mu)\, U_\mu^{\dagger {\rm adj}} \right], \tag{2.4}$$

where $U_\mu^{\rm adj}$ is the adjoint representative of U_μ, and κ is the usual hopping parameter, related to the bare quark mass by

$$m_0 = \frac{1}{2\kappa} - 4\,. \tag{2.5}$$

Periodic boundary conditions on both gauge and fermion fields have been built into the form of D_W. Throughout this paper we set $N_f = 2$.

The theory has a Z_N^4 center symmetry, under which

$$U_\mu \longrightarrow z^{n_\mu} U_\mu\,, \tag{2.6}$$

where $z = \exp(2i\pi/N)$ and $0 \le n_\mu < N$ are integers. Note that $U_\mu^{\rm adj}$ is invariant under this transformation, so that the fermion action is also invariant. There is also the single-site version of the gauge symmetry

$$U_\mu \longrightarrow \Omega U_\mu \Omega^\dagger \qquad [\Omega \in SU(N)]\,. \tag{2.7}$$

Finally, there is an $SO(4)$ flavor symmetry, most easily seen by writing the action in terms of four Majorana fields.[5]

If reduction holds, this single-site theory is equivalent, when $N \to \infty$, to a theory that has any number of lattice sites L_μ in each of the periodic directions $\mu = 1, 2, 3, 4$, including the case of $L_\mu = \infty$. The action of the $L_\mu > 1$ theories has the same form except that U, ψ, and $\bar\psi$, are now fields having a site index, $S_{\rm gauge}$ contains a sum over the position of the plaquettes, and D_W connects fermion fields at adjacent sites. We stress that an important feature of reduction is that it relates the single-site and infinite-volume theories having the same bare parameters, b and κ.

We recall some important properties of the infinite-volume theory, since these will be inherited by the single-site theory if reduction holds. First, the theory is asymptotically free—$N_f > 11/4$ fermions are required to change the sign of the first coefficient of the β-function. Second, although the bare quark mass vanishes when $\kappa = 1/8$, this critical value of κ is additively renormalized because Wilson fermions do not preserve chiral symmetry. The critical value is shifted to $\kappa_c(b) > 1/8$, and the physical quark mass becomes

$$m_{\rm phys} = \frac{1}{a}\left(\frac{1}{2\kappa} - \frac{1}{2\kappa_c}\right)\,. \tag{2.8}$$

Here we have introduced the lattice spacing, a, which can be determined, in principle, by fixing the value for a physical scale, such as a particle mass. Since the theory is asymptotically free at short distances, one approaches the continuum limit ($a \to 0$) by sending $b \to \infty$, and in this limit $\kappa_c(b) \to 1/8$.

The nature of this critical line depends on the infrared behavior of the theory. One possibility is that the theory lies below the conformal window, so that chiral symmetry is spontaneously broken, much as in QCD. Then, for κ near κ_c, one can study the long-distance behavior and vacuum structure of the lattice theory using chiral perturbation theory (ChPT). In particular, close to the continuum limit, one can use a modified ChPT which includes discretization effects [20]. For adjoint fermions, the symmetry breaking pattern differs from that in QCD, and is $SU(4) \to SO(4)$. The required generalization of the analysis of Ref. [20] has been given in Ref. [21]. One finds that, as in QCD, there are two possible scenarios: either there is a first-order transition line, at which the degenerate pseudo-Goldstone "pions" attain their minimal, non-zero mass, or there are two second-order lines, along which the pions are massless, and between which there is an Aoki-phase [22]. Within the Aoki-phase, the $SO(4)$ vector symmetry is broken.[6] The width of the Aoki-phase is $\propto a^3$, and thus shrinks rapidly as one approaches the continuum limit.

A different possibility for the critical line arises if the massless theory is conformal in the infrared, i.e. if there is an infrared fixed point. There is growing numerical evidence that this is the situation in the $N = 2$ theory. For this theory, the simulations of Refs. [25] and [26] map out parts of the phase diagram. In particular,

---

[5] In the continuum this symmetry becomes an $SU(4)$ symmetry, but, with our choice of fermion discretization, only its $SO(4)$ subgroup remains an exact symmetry of Eq. (2.1)).

[6] We note for completeness that Refs. [23, 24] have recently raised concerns about the consistency of the "first-order scenario."

there is single, second-order transition line emanating from ($b = \infty$, $\kappa = 1/8$), while for $b \lesssim 1/4$ the line becomes a first-order transition. (A similar picture holds for an improved fermion action, but in this case the second-order line extends to stronger coupling [27].) This is not established definitively, and also does not directly apply to the $N = \infty$ theory that we are interested in. Nevertheless, this possibility provides a quite different phase diagram than that which applies when one is outside the conformal window. One of our aims is to see which possibility holds at $N = \infty$ (assuming that reduction holds).

III. SIMULATION ALGORITHM

We simulate the single-site theory using the hybrid Monte-Carlo (HMC) algorithm [28]. Integrating out the fermions leads to

$$Z_{\rm AEK} = \int \prod_\mu DU_\mu e^{S_{\rm gauge}} \det(D_W)^2 \,. \tag{3.1}$$

As usual, γ_5 hermiticity implies that $\det(D_W)$ is real, so we can write

$$\det(D_W)^2 = \det(D_W D_W^\dagger) = \det(Q^2) \,, \tag{3.2}$$

where $Q = D_W\gamma_5 = Q^\dagger$ is the Hermitian Wilson-Dirac operator. Since Q^2 has positive eigenvalues, we can represent its determinant using pseudofermions. Introducing momenta conjugate to the link variables, we end up with the HMC Hamiltonian

$$H = \frac{1}{2}\sum_\mu {\rm tr}\,(P_\mu^2) - 2Nb\sum_{\mu<\nu} {\rm ReTr} U_{\mu\nu}^{\rm plaq} + \phi^\dagger Q^{-2}\phi \,. \tag{3.3}$$

The P_μ are traceless hermitian $N \times N$ matrices, while the pseudofermion ϕ is complex, lives in the adjoint representation of $SU(N)$, and has an implicit Dirac index. It thus has $4(N^2-1)$ complex components.

In practice, we represent ϕ in color space as a traceless bifundamental, i.e. as a traceless $N \times N$ matrix, on which $U_\mu^{\rm adj}$ acts as

$$U_\mu^{\rm adj}\phi \longrightarrow U_\mu \phi U_\mu^\dagger \,. \tag{3.4}$$

In this way we do not need to explicitly construct $U_\mu^{\rm adj}$.[7] In fact, one could, in principle, keep the trace of ϕ, since the singlet field that it represents has no impact on the dynamics. In particular, one can show that, in exact arithmetic, the molecular dynamics (MD) trajectories that are followed are identical with or without ${\rm tr}\,\phi$ included, as is the change in H. We find, however, that the number of CG iterations required for a given accuracy is larger if ${\rm tr}\,\phi$ is included, presumably because one has to do some work to find the solution for the singlet part. Thus we always set ${\rm tr}\,\phi = 0$.

Our implementation of the HMC algorithm is standard. We invert Q^2 using the conjugate gradient (CG) algorithm, with a weaker stopping criterion during the MD evolution than for the accept-reject step. We require that the residue, $r = b - Q^2 x$, with b the source, satisfies $|r|^2/|b^2| < 10^{-5}$ during MD evolution, finding that any further increase of the cut-off leads to a drop in the acceptance. For the accept-reject step we use $|r|^2/|b^2| < 10^{-15}$, which makes the error in ΔH negligible. Our CG always starts from a vanishing guess, $x_0 = 0$, which assures reversibility of the trajectory. We use trajectories of unit length, and adjust the step size to attain acceptances of $0.6 - 0.85$.

In deriving the gluonic force, one must account for the fact that each link appears twice in each plaquette. Nevertheless, the final result has the standard large-volume form:

$$\dot{P}_\mu^U = iNb\sum_{\nu\neq\mu} U_\mu \left[U_\nu U_\mu^\dagger U_\nu^\dagger + U_\nu^\dagger U_\mu U_\nu\right] + h.c. \tag{3.5}$$

[7] We thank Simon Catterall for stressing this point to us.

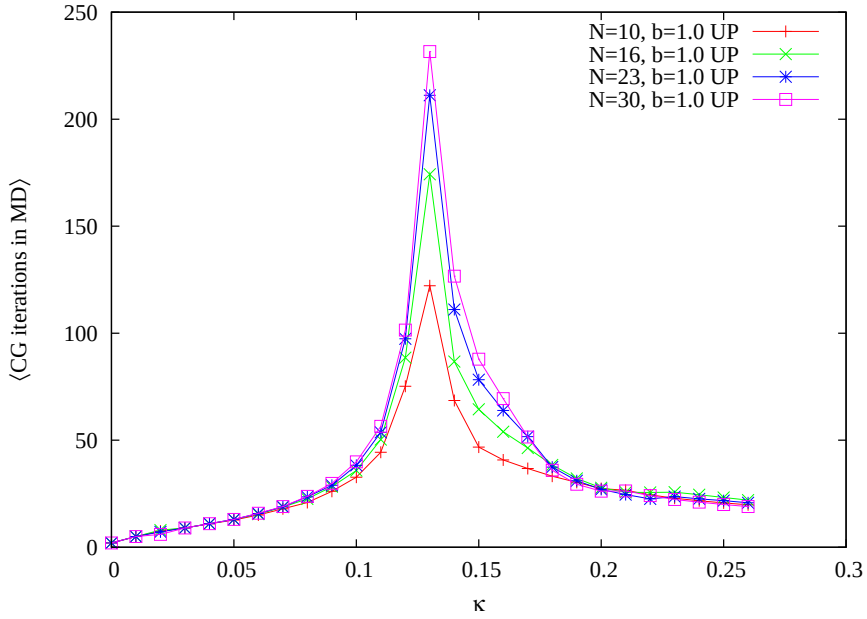

FIG. 1. Average number of CG iterations in the MD updates for various N as a function of κ at $b = 1.0$. Results are from UP scans.

The fermionic force is

$$\dot{P}_\mu^\phi = i\kappa \Big\{ (\gamma_5 + \gamma_\mu\gamma_5)_{\alpha\beta} \left[\psi_\beta U_\mu \chi_\alpha^\dagger U_\mu^\dagger - U_\mu \chi_\alpha^\dagger U_\mu^\dagger \psi_\beta\right] - (\gamma_5 - \gamma_\mu\gamma_5)_{\alpha\beta} \left[U_\mu \psi_\beta U_\mu^\dagger \chi_\alpha^\dagger - \chi_\alpha^\dagger U_\mu \psi_\beta U_\mu^\dagger\right] \Big\} + h.c. \tag{3.6}$$

where α and β are Dirac indices, $\chi = Q^{-2}\phi$, and $\psi = Q\chi$. Both forces maintain the tracelessness of P_μ.

We now discuss the scaling of CPU time with N, which is a key factor in determining how large one can take N. The core operation—multiplication of $N \times N$ matrices—scales as N^3. The use of the bifundamental form of U_μ, rather than the adjoint, is crucial here, reducing the scaling from N^4 to N^3, as pointed out in Ref. [19]. The next contribution to the overall scaling comes from the number of CG iterations, N_{CG}. This turns out to depend on the proximity to the critical line. An example is shown in Fig. 1, for the stopping criteria given above. Away from the critical line, N_{CG} is independent of N, while near the line it grows roughly like $N^{1/2}$. The third ingredient is the inverse step size, or equivalently the number of MD steps (N_{MD}) per trajectory (for a given acceptance rate). We find that, to good approximation, this grows linearly with N. Thus, for trajectories of unit length, CPU time scales as $\sim N^4$ away from the critical line, and roughly as $\sim N^{4.5}$ near to the line. Both scalings are considerable improvements over that for the Metropolis algorithm used in Ref. [8], which is N^6 for each SU(2) subgroup update and N^8 for an entire update. On the other hand, our scaling is not as good as the estimate of $N^{3.5}$ given in Ref. [19], which assumed $N_{MD} \propto N^{1/2}$ and that N_{CG} is independent of N, and explicitly excluded the possible effects of critical slowing down.

We have done both horizontal (fixed b) and vertical (fixed κ) scans in the $b - \kappa$ plane, studying the ranges $\kappa = 0 - 0.6$ and $b = 0.05 - 200$, although our main focus has been on the smaller ranges $\kappa = 0 - 0.26$ and $b = 0.35 - 1.0$. We use $N = 10 - 30$ in these scans. Rather than quote a complete set of run parameters we give a representative example. We have, for $b = 0.35$, 0.5, 0.75 and 1.0, used 27 values of κ ($0.0 - 0.26$ in steps of 0.1). At each κ, we start from the "configuration" output from the previous value, thermalize for 500 trajectories, and then run for 7500 ($N = 10$), 5000 ($N = 16$), 2000 ($N = 23$) or 1000 ($N = 30$) trajectories during which we make measurements every 5 trajectories and store the configurations every 50. Each scan is

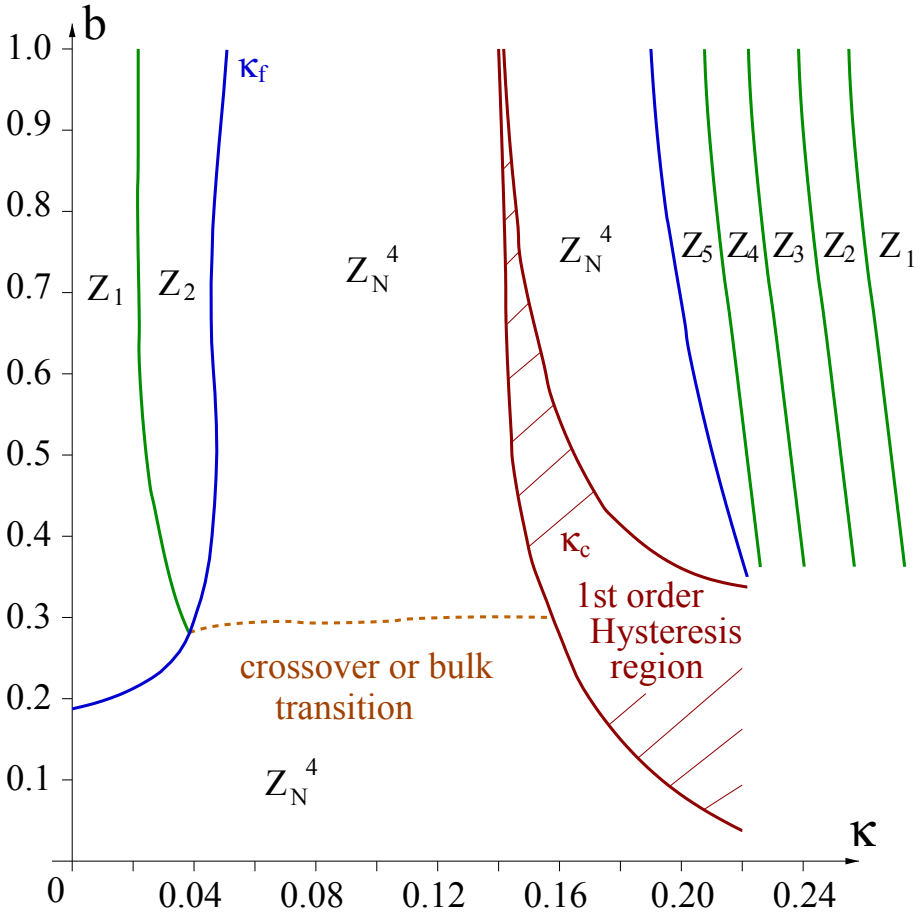

FIG. 2. Sketch of phase diagram for the $N_f = 2$ AEK model in the $\kappa - b$ plane for $N \approx 30$. Note that the $\kappa = 0$ axis is the EK model. The positions of phase boundaries are approximate, and depend somewhat on N. The shaded region at κ_c indicates the uncertainty in the position of what appears to be a first-order transition due to hysteresis. Within each region we note the subset of the Z_N^4 center symmetry that is unbroken, with Z_1 indicating complete breakdown. The center symmetry is unbroken in the hysteresis region. The detailed symmetry-breaking pattern for large κ is representative, and depends to some extent on N. For further discussion, see text.

done in both directions—the UP and DOWN scans denoting increasing or decreasing parameter values (either κ or b). To give an example of the CPU time required, the $b = 1.0$ UP scan took 33, 155, 342 and 618 CPU-hours of a single core on 3.0 GHz Intel Xeon processor, for $N = 10$, 16, 23 and 30, respectively. Our simulations have been done on local workstations and using up to 32 CPU cores on a computing cluster.

We have also done longer runs at several points in the $b - \kappa$ plane, in which we have gone up to $N = 53$. Details of these runs will be given below.

IV. PHASE DIAGRAM OF THE $N_f = 2$ AEK MODEL

In this section we present our main results, from which we deduce the phase diagram sketched in Fig. 2. The most important conclusion is that there is a "funnel" in which the center symmetry is unbroken, on either side of the first-order transition which we identify with κ_c. The diagram is qualitatively similar to that found for $N_f = 1$ [8].

A. Measured quantities

To study the gross features of the phase diagram, we calculate the average of the plaquette, u_p, defined by

$$u_p \equiv \frac{1}{6N} \sum_{\mu<\nu} Tr(U^{\rm plaq}_{\mu\nu}). \tag{4.1}$$

To study center symmetry breaking, we consider general "open loops":

$$K_n \equiv \frac{1}{N} {\rm tr}\, U_1^{n_1} U_2^{n_2} U_3^{n_3} U_4^{n_4}, \quad \text{with} \;\; n_\mu = 0, \pm 1, \pm 2, \ldots \tag{4.2}$$

where $U^{-n} \equiv U^{\dagger n}$. These loops transform non-trivially under the center symmetry, unless all four n_μ are integer multiples of N. They are thus order parameters for center-symmetry breaking.[8] The simplest choices, on which we focus, are the four Polyakov loops, $P_\mu = \frac{1}{N}{\rm tr}\, U_\mu$ and the 12 corner variables, $M_{\mu\nu} = \frac{1}{N}{\rm tr}\, U_\mu U_\nu$ and $M_{\mu,-\nu} = \frac{1}{N}{\rm tr}\, U_\mu U_\nu^\dagger$, with $\mu \neq \nu$.

As in the quenched Eguchi-Kawai model, the corner variables turn out to be particularly useful because they are sensitive to partial symmetry breaking [29]. We illustrate this with simple examples. First, if $U_\mu = \mathbf{1}$ for all μ, then all the Polyakov loops and corner variables are unity. This corresponds to complete breaking of the center symmetry. If instead

$$\forall \mu: \quad U_\mu = {\rm diag}\left(\underbrace{1, \ldots, 1}_{N/2 \text{ entries}}, \underbrace{-1, \ldots, -1}_{N/2 \text{ entries}} \right) \tag{4.3}$$

(where we have assumed that N is divisible by 4, so that $\det U_\mu = 1$), then the Polyakov loops vanish, while all corner variables are unity. In this case, there is a unbroken subgroup: both $\langle P_\mu \rangle$ and $\langle M_{\mu,\pm\nu} \rangle$ are invariant under the Z_2 subgroup of Z_N^4 generated by

$$\forall \mu: \quad U_\mu \to \pm U_\mu. \tag{4.4}$$

The U_μ themselves are invariant under the combination of Eq. (4.4) and a gauge transformation, the latter being the similarity transformation which interchanges the first $N/2$ diagonal entries with the second $N/2$ entries.

Such partial symmetry breaking can be discussed in a gauge invariant way by considering the eigenvalues of link matrices. For each link we can write

$$U_\mu = W_\mu \Lambda_\mu W_\mu^\dagger, \quad W_\mu \in SU(N), \tag{4.5}$$

with Λ_μ containing the eigenvalues:

$$\Lambda_\mu = {\rm diag}\left(e^{i\theta_\mu^1}, e^{i\theta_\mu^2}, \ldots e^{i\theta_\mu^N} \right). \tag{4.6}$$

Gauge transformations can permute the eigenvalues, but not change their values. Center-symmetry transformations change the eigenvalues by a uniform translation: $\theta_\mu^a \longrightarrow \theta_\mu^a + 2\pi n_\mu/N$. Thus a direct way of looking for certain symmetry breaking schemes, and understanding their nature, is to look at the distributions of the θ_μ. For example, unbroken center symmetry implies a distribution which is invariant under translations by $2\pi n/N$. Partial symmetry breaking occurs when a subgroup of such translations is unbroken. In the first example above, the eigenvalues are all clumped, and all translation symmetries are broken. In the second example, the eigenvalues form two clumps, and translation by π remains a symmetry.

We use the link eigenvalues in Sec. IV E, plotting histograms and considering the correlations between links in different directions.

---

[8] We have used $-5 \leq n_\mu \leq 5$ to keep the quantity of data manageable. This has the disadvantage that the traces are then insensitive to symmetry breaking such as $Z_N^4 \to Z_{10}$. Histograms of link eigenvalues, to be discussed below, are, however, sensitive to such symmetry breaking.

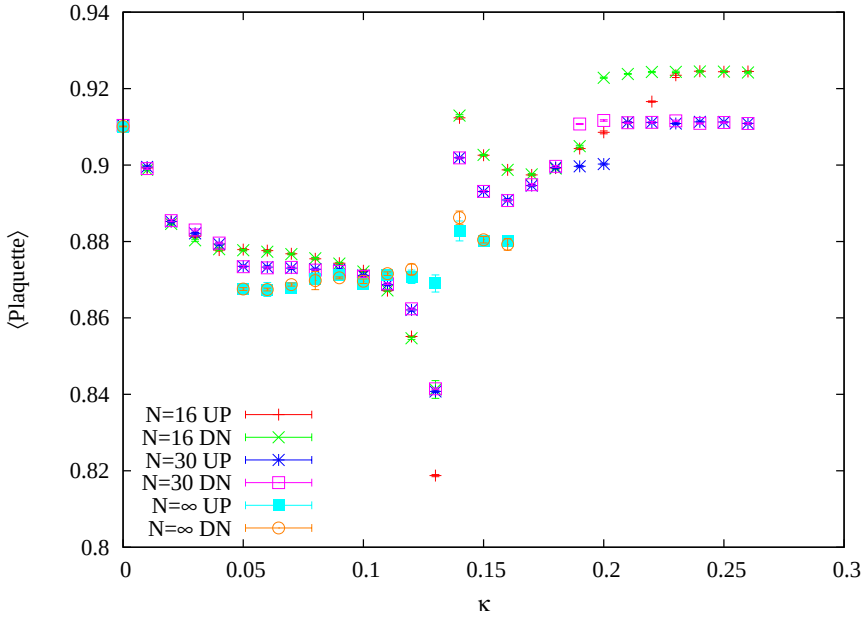

FIG. 3. Scans (both UP and DOWN) of the average plaquette at $b = 1.0$ for $N = 16$ and 30. The results of an extrapolation to $N = \infty$ (described in the text) are shown in the central region.

B. Scans at moderate coupling ($b \leq 1$)

In this section we use scans of the plaquette, Polyakov loops and corner variables to map out the gross features of the phase diagram.

The most interesting values of b are roughly $0.35 - 1.0$; this was the range studied in the $N_f = 1$ model [8]. For $N = 3$, this corresponds to $\beta = 6/g^2 = 6.3 - 18$, a range running from couplings similar to those used in large-volume simulations to very weak coupling. We have made detailed scans at $b = 0.35$, 0.5, 0.75 and 1.0. That at $b = 0.35$ shows a great deal of structure that is hard to analyze (including large hysteresis and the influence of a bulk transition), while that at $b = 0.75$ interpolates between the results at $b = 0.5$ and 1.0. Thus we show, in Figs. 3 and 4 respectively, scans of the plaquette at $b = 1.0$ and 0.5. We have simulated with $N = 10$, 16, 23 and 30, but, for the sake of clarity, show results only for $N = 16$ and 30. We also show, in the central region, an approximate estimate of the result at $N = \infty$, obtained by fitting results at the four values of N (or more values, if available) to $c_0 + c_1/N + c_2/N^2$. Such fits will be discussed in Sec. IV C.

The results at $b = 1$ show three main features: (i) a change in slope at $\kappa \approx 0.02$ (and possibly another at $\kappa \approx 0.05$), (ii) a jump at $\kappa = 0.13 - 0.14$, and (iii) a transition region at $\kappa \approx 0.2$. These correspond on the phase diagram of Fig. 2 to (i) the transition region from center-symmetry broken phases to the unbroken central region, (ii) the transition line at $\kappa_c \approx 0.13$, and (iii) the transition to the region of multiple broken phases for large κ. We focus first on the central feature, presenting our evidence concerning symmetry-breaking below. An important issue is whether the jump at finite N survives as a first-order transition at $N = \infty$. Our extrapolations suggest that it does: although the jump in the plaquette decreases with N, it appears to remain finite at $N = \infty$.

The conclusion of a first-order transition is clearer in the results at $b = 0.5$. These show the same qualitative features as for $b = 1$, but the jump in the plaquette is larger, and there is hysteresis for $N = 16$ and 30.[9]

[9] We note in passing a peculiar phenomenon we have seen for smaller values of N in the range we consider. At $N = 10$, the UP scans for $b = 0.5$ show, in the hysteresis region, points having average plaquettes with non-vanishing imaginary parts. This breaks the charge conjugation symmetry of the theory, and is reminiscent of results found in the twisted EK model [31]. It is because of these points that we do not have an extrapolated result for the UP scans at $\kappa = 0.15 - 0.17$ in Fig. 4. We suspect that this occurs only in metastable phases, and view it as a sign of the complicated vacuum structure of the single-site theory.

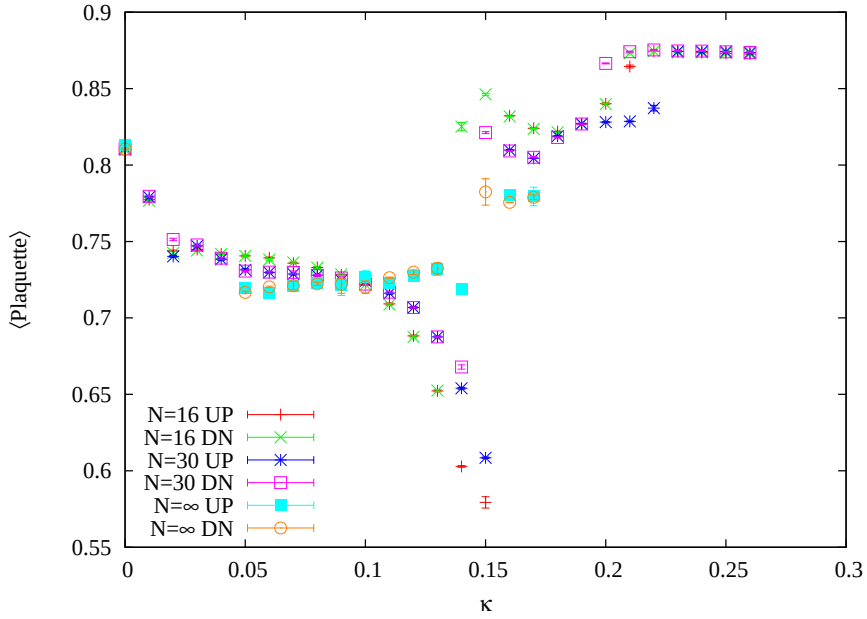

FIG. 4. As for Fig. 3 but for $b = 0.5$.

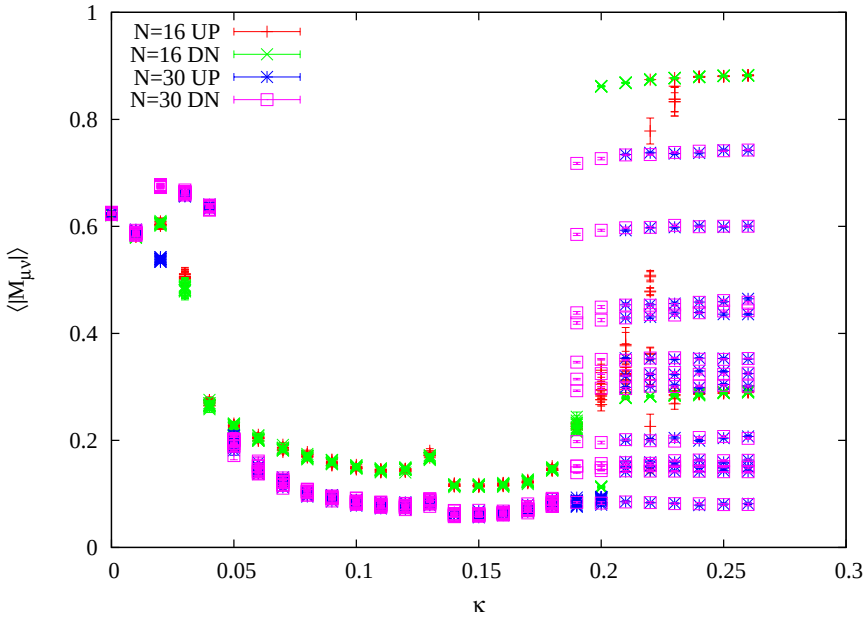

FIG. 5. Scans of the absolute values of corner variables for $b = 1.0$, for $N = 16$ and 30. Results for the 12 independent $|M_{\mu\nu}|$'s are shown separately.

To study center symmetry breaking, we first use scans of the absolute values of Polyakov loops and the corner variables. Both should vanish as $N \to \infty$ if the symmetry is unbroken. The corner variables are more informative and we show an example, for $b = 1.0$, in Fig. 5. Results for $0.35 \lesssim b < 1.0$ are qualitatively similar.

For both small and large κ, $\kappa \lesssim 0.05$ and $\kappa \gtrsim 0.19$, the corner variables indicate that the center symmetry

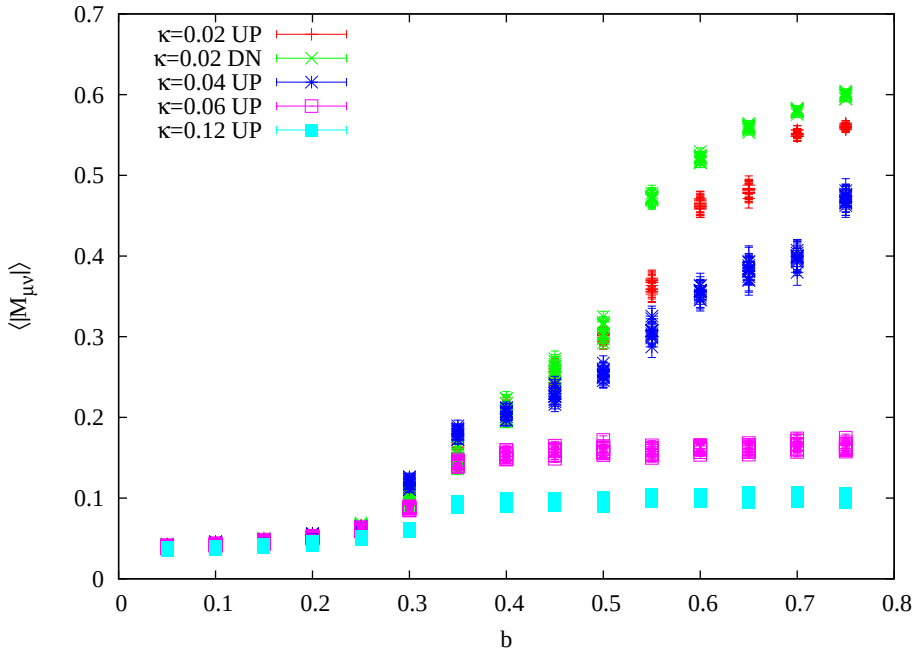

FIG. 6. Vertical scans of the absolute values of corner variables with $N = 23$ and for $\kappa = 0.02$, 0.04, 0.06 and 0.12. For $\kappa = 0.02$ both UP and DOWN runs are shown.

is broken. The nature of this breaking is clarified by the Polyakov loops, $|P_\mu|$, whose plots we do not show for the sake of brevity. For $\kappa \lesssim 0.02$ we find $|P_\mu|$ to be non-vanishing as $N \to \infty$, indicating that the center symmetry is completely broken. This is the Z_1 phase shown in Fig. 2. For $0.02 \lesssim \kappa \lesssim 0.05$ and $\kappa = 0.19 - 0.20$, however, $|P_\mu|$ are consistent with zero at $N = \infty$, indicating only partial symmetry breaking. The nature of this partial breaking can be elucidated using the distributions of P_μ and $M_{\mu\nu}$ in the complex plane, and using histograms of link eigenvalues. Some examples of the latter will be shown in Sec. IV E.

A key issue for reduction is the realization of center symmetry in the central funnel, $0.05 \lesssim \kappa \lesssim 0.18$. For the values of N used in the scans, we find no indication of symmetry breaking. Our evidence is as follows. Scatter plots of $\langle M_{\mu\nu} \rangle$ and $\langle P_\mu \rangle$ in the complex plane show a single distribution centered around the origin, with averages consistent with zero. Similarly, the higher-order traces, K_n, which we have evaluated at several positions inside the funnel, are all consistent with zero. Finally, histograms of link eigenvalues, examples of which are shown in Sec. IV E, are also consistent with the absence of symmetry breaking.

The other key question is whether the funnel remains of finite width as $N \to \infty$. We can see from Fig. 5 that the funnel narrows with increasing N. In particular, the lower edge of the funnel, which we call κ_f, increases from $\kappa_f \approx 0.03$ at $N = 10$ to $\kappa_f \approx 0.05$ at $N = 30$. To study this question further requires larger values of N, and we defer consideration until Sec. IV D.

To complete the study of the phase diagram we have done several vertical scans with $N = 16$, 23 and 30. We show an example of the results in Fig. 6, which displays the $\langle |M_{\mu\nu}| \rangle$ for $N = 23$ and $\kappa < \kappa_c$. For all κ, there is no indication of symmetry breaking at strong coupling, $b \lesssim 0.3$, just as for the EK model. There are possible transitions, however, as we increase b. For example, at $\kappa = 0.02$ we see two transitions: one at $b \approx 0.3$ and a second at $b \approx 0.55$. The first is from a center symmetric phase to one in which both Polyakov loops and corner variables are non-vanishing, consistent with complete symmetry breakdown. The second is to a phase with large corner variables and smaller Polyakov loops, which we interpret as a partially broken phase. This is the same "Z_2" phase apparent in Fig. 5 for $\kappa = 0.02 - 0.04$.

For all other κ there is no hysteresis, so we show only UP scans. At $\kappa = 0.04$, we see only a single transition, at $b \approx 0.3$, and this is directly to a partially broken phase with only $\langle |M_{\mu\nu}| \rangle$ non-zero. For higher κ, however, the symmetry is unbroken on both sides of the jump at $b \approx 0.3$, and we interpret this as a bulk transition. It is unclear, however, whether this corresponds to a phase transition or a crossover as $N \to \infty$.

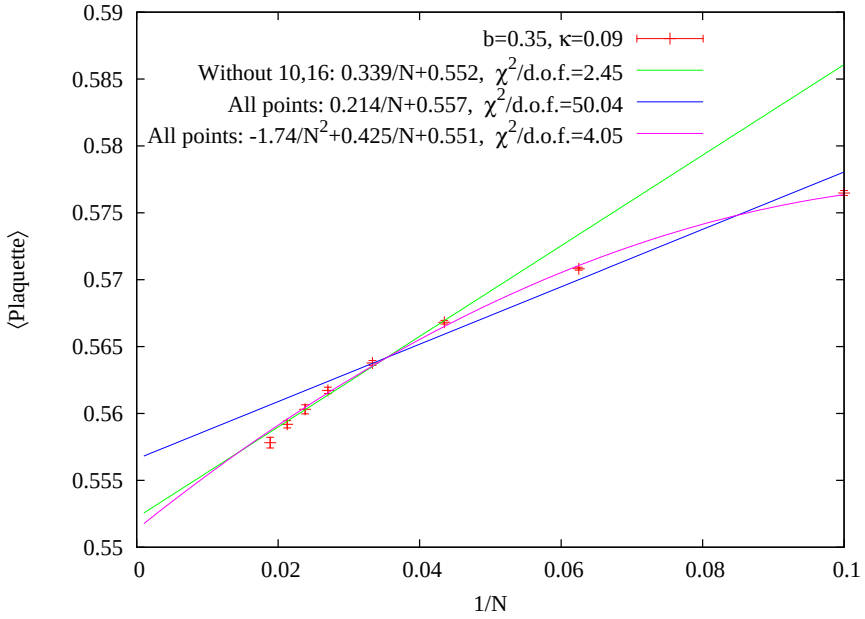

FIG. 7. Plaquette vs. $1/N$ at $b = 0.35$, $\kappa = 0.09$, showing various fits.

Vertical runs at higher values of κ fill in gaps left by the horizontal scans, and are part of the input which leads to the phase diagram of Fig. 2. For the sake of brevity, however, we do not show any plots here.

C. Scaling of the plaquette, $\langle|P_\mu|^2\rangle$, $\langle|M_{\mu\nu}|^2\rangle$

In order to study the key question of whether the symmetry unbroken funnel remains as $N \to \infty$, we have extended the calculations to larger values of N at several several values of b and κ.

We begin by looking at the average plaquette. If reduction holds, then, away from κ_c, the single-site theory is equivalent at large N to a large-volume lattice theory with quarks having physical masses of $O(1/a)$. The long-distance physics of such a theory is that of a pure-gauge theory with action modified from the pure Wilson form by fermionic effects. If κ is much smaller than κ_c, these modifications should be small, since they are proportional to powers of the small quantity κ (as can be seen using the hopping parameter expansion). The large-volume theory is thus close to the pure-gauge theory with Wilson action. We can therefore make the semi-quantitative prediction that, near the lower boundary of the funnel, κ_f, the average plaquette should lie close to the large-volume, pure-gauge (Wilson action) value, but depart from that value as one approaches κ_c. On the other side of the transition, however, we do not expect the plaquette to tend to this same value as $\kappa - \kappa_c$ increases. This is because κ is now larger, so the action differs more significantly from the pure-gauge Wilson form.

Figures 3 and 4 show that the plaquette has considerable dependence on N, with the slope of this dependence varying with κ. We show in Fig. 7 an example of an extrapolation in which the plaquette decreases with N, and in Fig. 8 an example in which it increases. Results are for $N = 10 - 53$ and are plotted versus $1/N$. We use this variable because we have found that we cannot obtain a reasonable fit without taking the leading correction to be proportional to $1/N$ (rather than $1/N^2$). Examples of fits to $c_0 + c_1/N$ and $c_0 + c_1/N + c_2/N^2$ are shown in the figures, fitting either to all the data or dropping the two lowest values of N. We find that fits of $c_0 + c_1/N$ to the highest six values of N are tolerable (probability $p \gtrsim 0.04$) for all choices b and κ that we have considered, and use such fits to obtain the results given in Table I.

The results for the plaquette at $N = \infty$ are in striking agreement with the semi-quantitative prediction explained above. In particular, for $\kappa = 0.06$ and 0.09 they are consistent with the pure-gauge large-volume

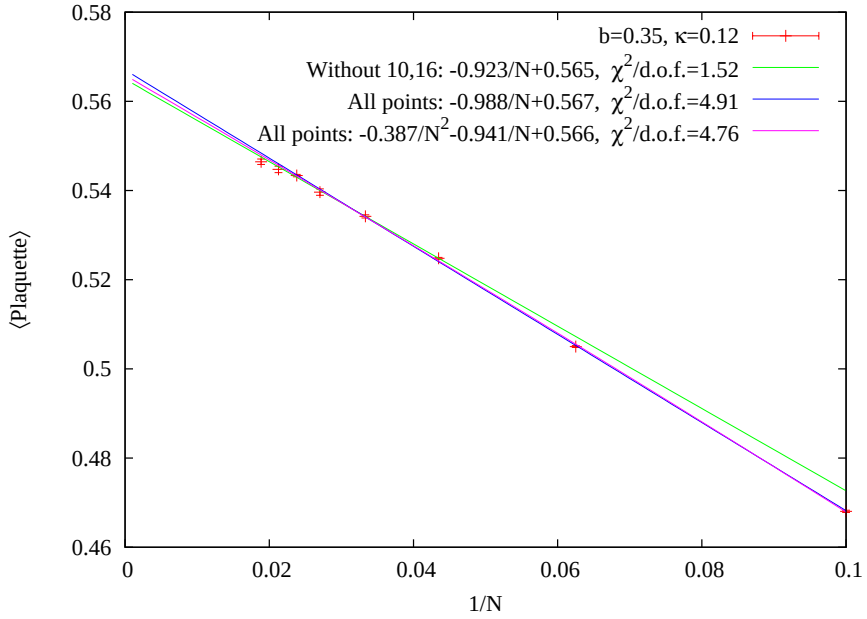

FIG. 8. As in Fig. 7 but for $\kappa = 0.12$.

b	κ	$\chi^2/d.o.f.$	c_1	c_0	pure-gauge value
0.35	0.06	1.8	0.75(4)	0.549(1)	0.550
0.35	0.09	2.4	0.34(4)	0.552(1)	0.550
0.35	0.12	1.5	-0.92(3)	0.565(1)	0.550
1.0	0.06	0.2	0.120(3)	0.8694(1)	0.8692
1.0	0.09	1.1	0.076(3)	0.8697(1)	0.8692
1.0	0.12	0.6	-0.248(4)	0.8709(1)	0.8692
1.0	0.15	2.3	0.39(1)	0.8795(4)	0.8692

TABLE I. Results from large-N extrapolation of plaquette expectation values. Extrapolations are done using a fit of $c_0 + c_1/N$ to results at $N = 23$, 30, 37, 42, 47 and 53. Results for c_0, c_1 and $\chi^2/d.o.f.$ are given, with errors being statistical. Systematic errors (from different choices of fit function) are a few times larger than the statistical errors. Our best estimate of the pure-gauge large-volume expectation value is also quoted. The $b = 1$ value is obtained from Ref. [8], while that at $b = 0.35$ is obtained from the $N = 8$ pure gauge result at $b = 0.3504$ from Ref. [30].

results, while for $\kappa = 0.12$ (close to κ_c) they begin to differ. Thus, looking back at the scans of the plaquette in Figs. 3 and 4, we see that the extrapolation to $N = \infty$ leads to an almost constant value between the onset of the funnel at $\kappa_f \approx 0.05$ and κ_c, with the value being close to that of the pure-gauge theory.

We also have results for a single point above κ_c: $\kappa = 0.15$ at $b = 1.0$. We find here that the extrapolated plaquette differs, with high significance, from that below κ_c. This is consistent with our semi-quantitative prediction, and also indicates that the first-order transition at κ_c survives the large N limit.

We now return to our numerical finding that the leading corrections to the plaquette scale as $1/N$. This result has also been found in the numerical studies of Ref. [11]. It differs from the naive expectation that, with fields in the adjoint irrep, corrections should be powers of $1/N^2$. We find, however, that fits to $c_0 + c_2/N^2 + c_4/N^4$ are only possible with very large coefficients ($|c_2| \sim 10 - 20$, $|c_4| \sim 2500$) of alternating signs. We consider these fits unreasonable since we expect coefficients of $O(1)$.

In fact, there are (at least) two possible sources of $1/N$ terms. The first can be seen from the perturbative

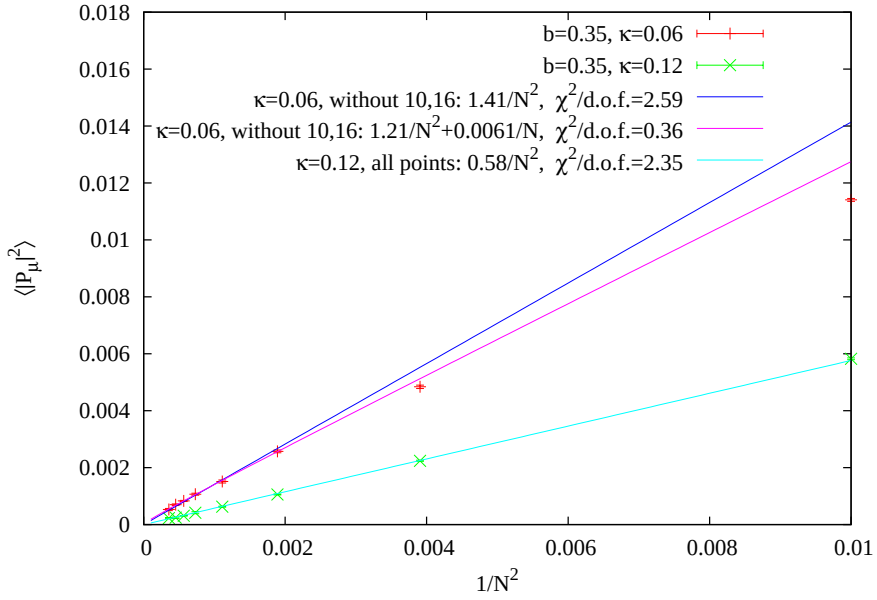

FIG. 9. $\langle|P_1|^2\rangle$ versus $1/N^2$ for $b = 0.35$ and $\kappa = 0.06$ and 0.12, along with a variety of fits.

result for the plaquette when one has a center-symmetric vacuum [4]

$$u_p = 1 - \frac{1}{8b}(1 - 1/N) + O(1/b^2)\,, \tag{4.7}$$

which manifestly contains a $1/N$ correction.[10] This correction arises from the fact that in the decomposition (4.5) non-trivial fluctuations in W_μ lie in $SU(N)/U(1)^{N-1}$. In other words, the fluctuations must be off-diagonal, leading to the factor $N(N-1) = N^2(1-1/N)$. We expect that the one-loop form (4.7) should work reasonably well at $b = 1$ (as it does for c_0 in Table I) and that the predicted $1/N$ correction should be most applicable for the smallest values of κ (where fermionic contributions to the plaquette are minimized). Indeed the result for c_1 at $b = 1$, $\kappa = 0.06$ lies close to the prediction of $1/8$.

A second source for $1/N$ corrections are the "would-be zero modes" of the Wilson-Dirac operator D_W, which we discuss in more detail in Sec. V A. There are $4(N-1)$ of these (corresponding, as in the gauge case above, to the diagonal generators of SU(N) in perturbation theory), and they form an $O(1/N)$ fraction of the total number of modes. Unless the contribution of these modes is exactly canceled by an $O(1/N)$ contribution from the remaining $4(N^2 - N)$ eigenvalues, these modes can cause observables to depend on odd powers of $1/N$. Our results for the spectrum of D_W suggest that they play an important role in the dynamics for the values of b at which we simulate.

We now turn to the extrapolations of $\langle|P_\mu|^2\rangle$ and $\langle|M_{\mu\nu}|^2\rangle$. In the large-$N$ limit, these can be written, using factorization, as $|\langle P_\mu\rangle|^2$ and $|\langle M_{\mu\nu}\rangle|^2$, respectively, both of which vanish if the center symmetry is unbroken. Thus an important test of our tentative phase diagram is that $\langle|P_\mu|^2\rangle$ and $\langle|M_{\mu\nu}|^2\rangle$ extrapolate to zero within the funnel.

Ordinarily, corrections to factorization are proportional to $1/N^2$, but, in light of our experience with the plaquette, we might also see $1/N$ corrections. In Fig. 9 we plot $\langle|P_1|^2\rangle$ versus $1/N^2$ for $b = 0.35$ and two values of κ. There is qualitative agreement with a $1/N^2$ fall-off for both κ's, but fits to a pure $1/N^2$ form, examples

[10] We thank Ari Hietanen for reminding us of this result.

Qty	b	κ	c_1	c_2	$\frac{\chi^2}{\text{d.o.f.}}$	c_0'	c_2'	$\frac{\chi'^2}{\text{d.o.f.}}$
$\langle\|P_1\|^2\rangle$	0.35	0.06	0.006(1)	1.21(6)	0.36	$9(1)\times10^{-5}$	1.31(1)	0.39
$\langle\|P_1\|^2\rangle$	0.35	0.09	0.0014(9)	0.73(3)	0.67	$2(1)\times10^{-5}$	0.76(2)	0.73
$\langle\|P_1\|^2\rangle$	0.35	0.12	0.001(3)	0.57(3)	0.82	$0(2)\times10^{-5}$	0.56(1)	0.84
$\langle\|M_{12}\|^2\rangle$	0.35	0.09	0.152(5)	2.9(1)	0.42	0.0023(3)	5.3(4)	2.57
$\langle\|M_{12}\|^2\rangle$	0.35	0.12	0.036(6)	3.5(2)	1.0	$5(1)\times10^{-4}$	4.1(2)	1.2
$\langle\|P_1\|^2\rangle$	1.0	0.06	−0.0001(3)	1.17(1)	0.025	$-1(3)\times10^{-6}$	1.17(1)	0.025
$\langle\|P_1\|^2\rangle$	1.0	0.09	−0.0003(4)	0.70(1)	1.2	$-5(6)\times10^{-6}$	0.70(1)	1.2
$\langle\|P_1\|^2\rangle$	1.0	0.12	−0.0010(3)	0.55(1)	0.60	$-1.4(4)\times10^{-5}$	0.54(1)	0.58
$\langle\|M_{12}\|^2\rangle$	1.0	0.06	0.69(3)	-1.6(7)	0.58	0.010(1)	9(2)	2.7
$\langle\|M_{12}\|^2\rangle$	1.0	0.09	0.0053(7)	6.1(2)	0.99	$8(2)\times10^{-4}$	6.9(3)	1.7
$\langle\|M_{12}\|^2\rangle$	1.0	0.12	0.01(1)	5.5(4)	0.4	$0(1)\times10^{-4}$	5.4(2)	0.41

TABLE II. Results from fits to the large-N behavior of $\langle|P_1|^2\rangle$ and $\langle|M_{12}|^2\rangle$. Fits are to $N = 23$, 30, 37, 42, 47 and 53 using $f_1(N) = c_1/N + c_2/N^2$ and $f_2(N) = c_0' + c_2'/N^2$, showing statistical errors.

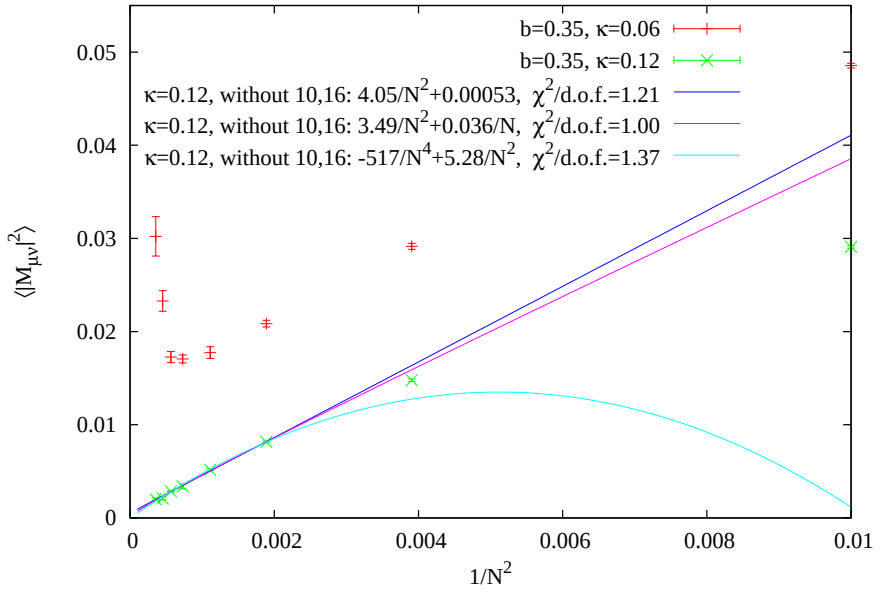

FIG. 10. As for Fig. 9 but for the corner variable $|M_{12}|^2$. Only fits to $\kappa = 0.12$ are shown.

of which are shown in the figure, have low confidence-levels. Satisfactory fits (one example of which is shown) can be found by adding a $1/N$ term and dropping the lowest two values of N.

Results from such fits, for all the values of κ and b at which we have done runs up to $N = 53$, are collected in Table II. The fits to $\langle|P_1|^2\rangle$ all have reasonable confidence levels. The coefficient of the $1/N$ term is small in all cases, and in fact is consistent with zero (within $\sim 3\sigma$) except for $b = 0.35$, $\kappa = 0.06$. We also show results of fits to a constant plus $1/N^2$ term. The fits are of very similar quality, and the constant turns out to be very small, and consistent with zero except, again, at $b = 0.35$, $\kappa = 0.06$. We conclude, aside from this one point near to the edge of the funnel, that the behavior of Polyakov loop is consistent with the hypothesis that reduction holds in the funnel.

Turning to the corner variables, examples of which are shown in Fig. 10 with full results collected in the Table, we find a surprising result: at $b = 0.35$, $\kappa = 0.06$, $\langle|M_{12}|^2\rangle$ starts to increase once N exceeds 40, and clearly does not extrapolate to zero. The simplest interpretation of this result is that the center symmetry is broken for $N \gtrsim 40$. There is, however, no other evidence for such symmetry breaking. In particular, the

distributions of the $M_{\mu\nu}$ and P_μ are approximately uniform around the origin, the traces K_n of Eq. (4.2) are all consistent with zero, and the link eigenvalues (to be discussed below) are distributed uniformly.

Instead, our favored interpretation is that the increase in $\langle|M_{12}|^2\rangle$ with N is due to the lower edge of the funnel, κ_f, increasing with N. This increase can be seen (albeit for $b = 1$) in Fig. 5 by comparing the results at $N = 16$ and 30. It is quite possible that, for $b = 0.35$, as N increases, κ_f approaches 0.06, possibly exceeding this value for $N > 53$. This would lead to the observed increase in $\langle|M_{12}|^2\rangle$ since this quantity increases as one approaches the transition (as can be seen in Fig. 5). This could also explain why our fits to $\langle|P_1|^2\rangle$ were less satisfactory at $b = 0.35$, $\kappa = 0.06$.

For all the other values of κ that we have considered $\langle|M_{12}|^2\rangle$ decreases monotonically with N. This is exemplified by the $\kappa = 0.12$ results in Fig. 10. As for the Polyakov loops, a pure $1/N^2$ fit fails in most cases, but here we find (cf. Table II) that the addition of a $1/N$ term usually leads to a better fit than the inclusion of a constant. We also find that, in almost all cases, the required $1/N$ (or constant) term has a coefficient which differs significantly from zero. We have also done fits to $c_2/N^2 + c_4/N^4$ (an example is shown if Fig. 10) but the fits require very large coefficients having opposite signs, a fine-tuning which we consider unlikely to be the correct description. Overall, we think the most reasonable fits are those to $c_1/N + c_2/N^2$, because they have the highest confidence levels, and because we have seen in the plaquette that $1/N$ terms are needed.

The results presented so far are consistent with the funnel (in which center symmetry is unbroken) remaining of finite width as $N \to \infty$, so that reduction holds for masses up to $O(1/a)$. We cannot definitively draw this conclusion, however, because of the following scenario. Imagine that the funnel width vanishes (for any fixed b) as $N \to \infty$. Then, for each b, κ point in the putative funnel, symmetry breaking would occur at a (possibly large, but) finite, value of N. Nevertheless, there would be a finite range of N for which the symmetry is unbroken, within which the arguments for reduction hold. Appropriate variables (such as the plaquette) would equal infinite volume values up to corrections proportional to powers of $1/N$. Thus, within this range, it might appear that one can extrapolate to the symmetry-unbroken $N = \infty$ limit, but this would in fact not be the case. The results for the plaquette at $b = 0.35$, $\kappa = 0.06$ in Fig. 9 are an example of such misleading scaling, since we have strong evidence from the corner variables that $\kappa_f > 0.06$ at this b for large enough N.

D. N-scaling of the funnel width

In the light of the results in the previous subsections it is important to directly study the N dependence of the funnel width. We have done so by focusing on κ_f, the lower edge of the funnel. If we can show that κ_f remains below κ_c as $N \to \infty$, then the funnel remains open.

To investigate this issue we have done fine scans of the small κ region, an example of which is shown in Fig. 11. There are two phases before one enters the funnel: a Z_1 phase for $0 \leq \kappa \lesssim 0.02$ and a Z_2 phase from $0.02 \lesssim \kappa \lesssim 0.05$. The transition between the first and second phase shows significant hysteresis, while that between the second phase and the funnel does not.

Determining $\kappa_f(N)$ to high precision is a significant numerical challenge. We have thus focused on a single value of coupling, $b = 1$. For this b, Fig. 3 shows that κ_c lies in the range $0.13 - 0.14$. We have done very fine scans near the edge of the funnel (roughly $\kappa = 0.02 - 0.07$) with N up to 53, and find that the corner variables are the most useful in determining the transition. We are able to pin down the transition, conservatively, to about $\delta\kappa = \pm 0.001$. The transition from the funnel is to a Z_2 phase for most N (as in Fig. 11), but to a Z_3 phase for $N = 47$ and 53. The results are plotted against $1/N$ in Fig. 12, and show remarkable linearity (note that, as earlier, we have excluded $N = 10$ and 16—including them requires adding a $1/N^2$ term to obtain a satisfactory fit). Two fits are shown. The first is to $c_0 + c_1/N$, and has a very small χ^2/d.o.f., with a reasonable coefficient of $1/N$. It yields $\kappa_f(N = \infty) = 0.0655(5)$, a value far below κ_c. The second fit is to $\kappa_c + c_1/N + c_2/N^2$, with the intercept fixed to $\kappa_c = 0.125$. This fit is extremely poor, and it gets even worse for $\kappa_c = 0.13 - 0.14$. We have also done the corresponding fits to the alternative quantity $am_f = 1/2\kappa_f - 1/2\kappa_c$, using $\kappa_c = 0.125$ or 0.13, and find consistent results. We conclude that, at least at this value of b, the funnel has finite width when $N = \infty$, so that reduction holds.[11]

[11] Note that, if we use the linear fit, then the funnel at $b = 1$ passes $\kappa = 0.06$ when $N \approx 92$. Thus the successful extrapolations of

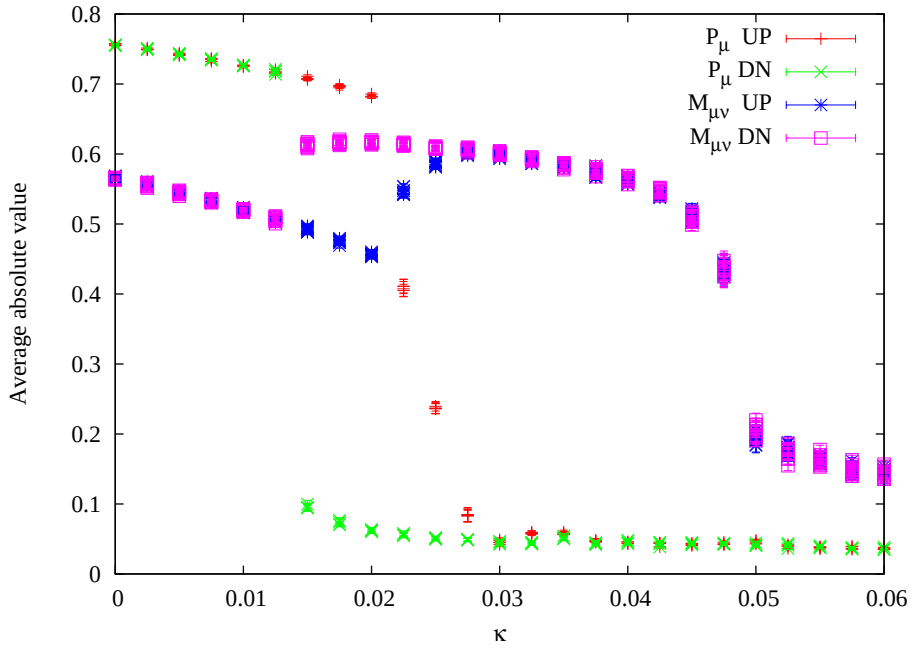

FIG. 11. Fine scans of absolute values of all Polyakov loops and corner variables in the low κ region, for $N = 30$ at $b = 0.75$.

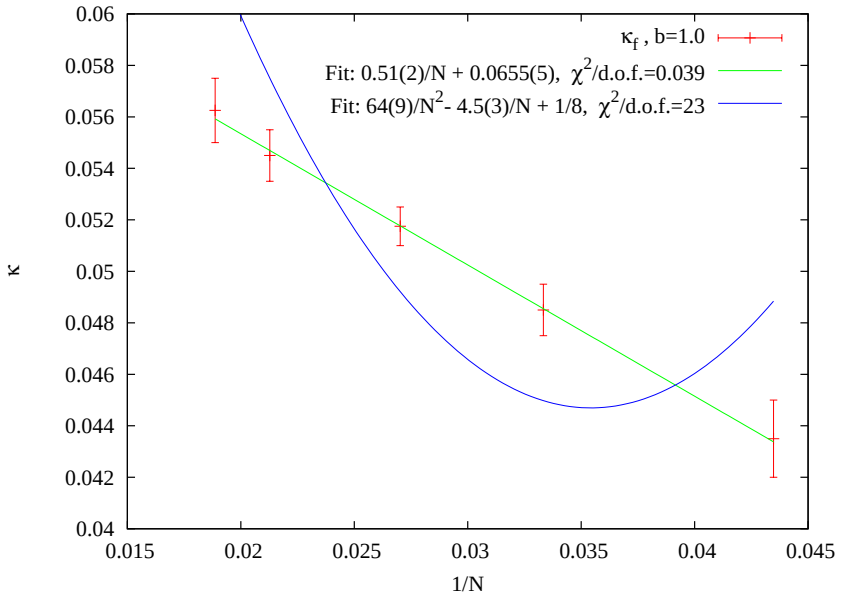

FIG. 12. The dependence of κ_f (lower edge of the funnel) on $1/N$ for $b = 1$. The fit functions are discussed in the text.

---

the plaquette, $\langle|P_1|^2\rangle$ and $\langle|M_{12}|^2\rangle$ for $b = 1$, $\kappa = 0.06$, presented in Tables I and II, are examples of the phenomenon described above in which reduction only holds for a window of values of N.

E. Distributions of link eigenvalues

We find that histograms of link eigenvalues provide very useful information on the nature of symmetry breaking on either side of the funnel. They are also sensitive to patterns of symmetry breaking in which both Polyakov loops and corner variables vanish, and thus provide a more stringent test that the symmetry is indeed unbroken in the funnel. In this section we present examples of the results that allow us to fill in the details of the phase diagram of Fig. 2.

We begin with an example of a histogram within the funnel, shown in Fig. 13(a). The eigenvalues are taken to have the range $-\pi < \theta_\mu^a \leq \pi$, and are collected in $3N$ bins of width $2\pi/(3N)$. Thus Z_N symmetry implies invariance under periodic translations by multiples of 3 bins. In fact the distribution is consistent with being uniform.[12]

When we move outside the funnel the attraction between eigenvalues leads to formation of clumps in the complex plane. The number of clumps k identifies the approximate remnant Z_k symmetry and generally decreases as we move away from the funnel. In Fig. 13 we provide several examples of clumping patterns. Figs. 13(b) and 13(c) present Z_1 and Z_2 phases in the small κ region while Figs. 13(d), 13(e) and 13(f) show Z_3, Z_4 and Z_5 phases in the large κ region. Note that the partial symmetry breaking can also be seen in the corner variables giving complex patterns (compare Fig. 5). Polyakov loops are much less sensitive to this partial symmetry breaking, since they almost vanish due to the approximate Z_k symmetry.

We find that the remnant symmetry is not always exact. For example, in Fig. 13(c) we have two clumps for $N = 23$ and in Fig. 13(d) we have three clumps for $N = 16$. Therefore the eigenvalues cannot be equally distributed between the clumps and the symmetry is only approximate. Even in Fig. 13(f), which shows five clumps for $N = 30$, we see that the clumps are not even and correspond to 7,6,7,4,6 eigenvalues, respectively. We also find that different runs can have different patterns of eigenvalue clumping, e.g. 7,7,6,6,4 versus 7,6,6,6,5, but that it is rare for the clumping to change during a run. Thus it appears that there are competing "vacua" which are not exactly related by center symmetry transformations.

To fully understand the symmetry breaking, we need to know whether there are correlations between the eigenvalues of different links. What we find is that, whenever the center symmetry is broken, the eigenvalues for all four links are highly correlated. To illustrate this, we use a case with three clumps which makes the results easy to visualize. Figure 14 shows the resultant clumping and correlations. Here we apply a gauge transformation which diagonalizes U_1 and orders the phases θ_1^a, and then look at the phases of the diagonal elements of $U_{2,3,4}$. These matrices are close to diagonal, so these phases are presumably close to those of their eigenvalues. Recall that there is no ambiguity in the ordering of the diagonal elements once we specify the order for U_1. The result shows that the clumps (of 6, 4 and 6), while being positioned at different angles, are almost completely correlated between all four links, and do not change during the Monte-Carlo evolution. Because of these correlations, the approximate remnant of the center symmetry for the parameters of Figs. 13(d) and 14 is Z_3, and not Z_3^4.

Once outside the funnel, the number of clumps decreases as we move to higher κ. We have extended some runs to $\kappa = 0.6$ and find that the UP scans end up in a two clump state, while the DOWN runs, which begin from an ordered start, begin with a single clump, and then have a transition, as κ is decreased, to two (well separated) clumps. In fact, the transition appears to occur in stages where more and more eigenvalues peel off from the initial clump. As κ is further decreased, the number of clumps increases until we enter the funnel and there is no longer any clumping. The largest number of clumps depends on N, and the largest we have observed is five, as shown in Fig. 13(f).

The changes in clumping for the large κ values, surveyed above, are qualitatively consistent with the arguments presented in Ref. [11] based on the one-loop free-energy for the link eigenvalues. Decreasing κ from a large value corresponds to reducing the quark mass am. For large am, gluonic interactions dominate the free energy, and lead to attraction, and thus a single clump. As am is reduced, the fermionic contributions lead to repulsion at large eigenvalue separations (corresponding to large momenta, so that the mass term is unimportant), while there remains attraction for small separations. This allows the possibility of two clumps.

[12] As a check on our code, we have calculated the distribution in the $b = 0$, $\kappa = 0$ limit, i.e. for the Haar measure on the links, and obtain the theoretically expected form, which is Z_N-invariant, but does oscillate within each Z_N segment, although the amplitude of the oscillations falls as $1/N$ [32].

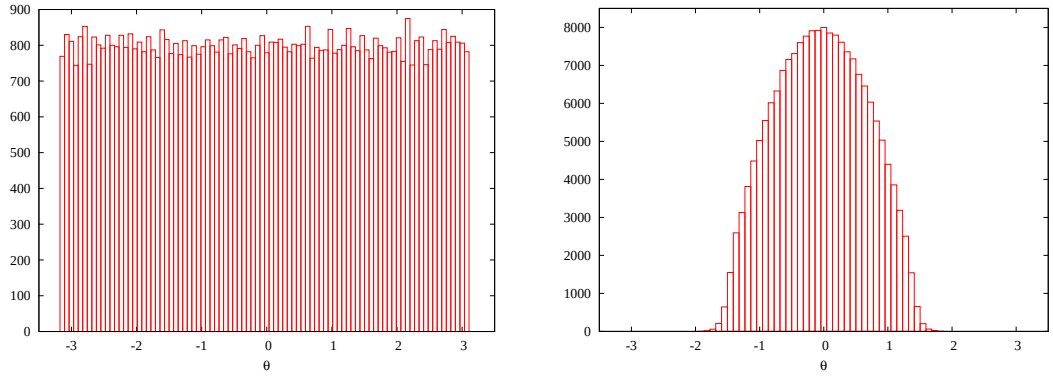

(a) $N = 30$, $b = 0.35$, $\kappa = 0.09$, 600 configs, all links

(b) $N = 23$, $b = 1.0$, $\kappa = 0.01$, 2000 configs, all links

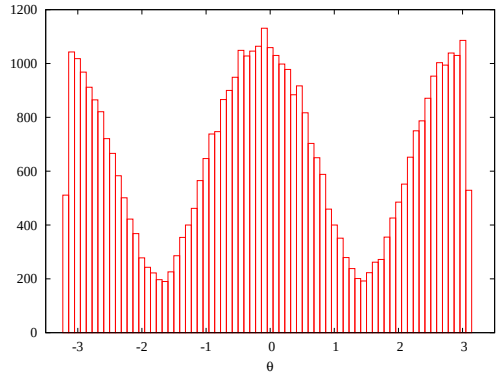

(c) $N = 23$, $b = 1.0$, $\kappa = 0.03$, 2000 configs, U_2 only

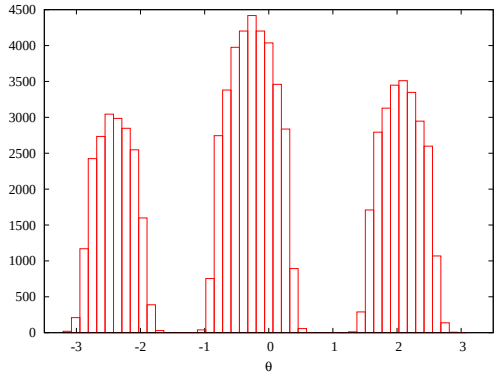

(d) $N = 16$, $b = 1.0$, $\kappa = 0.24$, 5000 configs, U_3 only

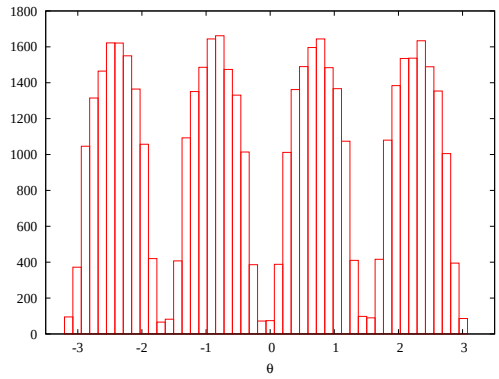

(e) $N = 16$, $b = 0.35$, $\kappa = 0.22$, 3000 configs, U_3 only

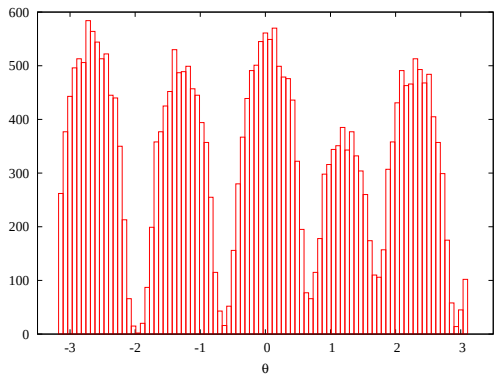

(f) $N = 30$, $b = 1.0$, $\kappa = 0.23$, 1000 configs, U_1 only

FIG. 13. Histograms of the phases θ_μ^a of the link eigenvalues. More details of the binning are discussed in the text.

Reducing am further the repulsion becomes important for smaller eigenvalue separations, and clumps are pulled apart into a greater number of stable clumps. At the same time, quantum fluctuations within each clump are always present, so that the clumps have a finite width (which is proportional to $b^{-1/4}$ for weak coupling). Eventually, as the number of clumps increases, the distance between the clumps is smaller than the widths, and the clumping is washed out.

We would expect a similar sequence of clumpings to occur as we increase κ from zero, since this also

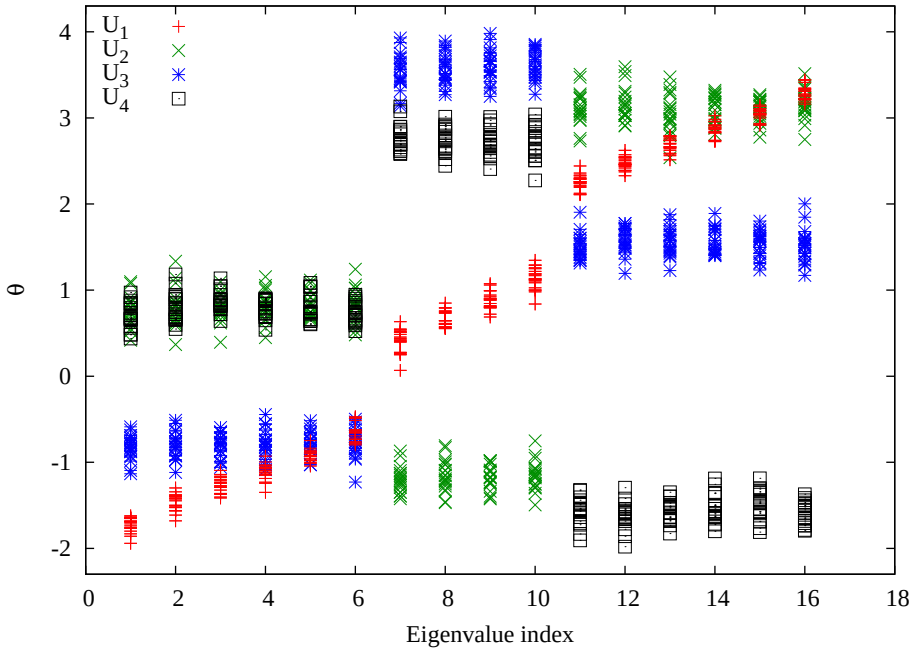

FIG. 14. Results for the phases of the diagonal elements of U_μ for 20 thermalized configurations at $N = 16$, $b = 0.35$ and $\kappa = 0.23$ on an UP scan. Phases are determined in a gauge such that U_1 is diagonal with the phases ordered. For further discussion, see text.

corresponds to reducing am. This is indeed what we observe, although the maximal number of clumps is smaller on this side of the funnel. For $N < 23$ we only find a Z_1 phase, for $23 \leq N < 47$ we see both a Z_1 and Z_2 phase (see Fig. 11), while for $N = 47$ and 53 we find Z_1, Z_2 and Z_3 phases. At larger values of b, the arguments of Ref. [11] imply that the maximal number of clumps should increase. Indeed, we do find that, as b increases, the Z_3 phase appears at smaller values of N.

F. Results at large b

The perturbative calculations of Refs. [9, 10] lead us to expect that the center-symmetry-unbroken funnel will close as $b \to \infty$, so that, in the continuum limit, reduction only holds for $m = 0$ (for $N \to \infty$). In addition, Ref. [11] makes a prediction for how rapidly the funnel should close: its width in am (and thus in κ) should be proportional to $b^{-1/4}$. This is because the width of each clump of link eigenvalues is predicted to scale to zero proportional to $b^{-1/4}$. A second prediction (which is explained in the previous subsection) is that, at the edge of the funnel, there should be multiple phases with differing numbers of clumps, and that the maximum number of clumps should increase with b (as long as N is large enough). In other words, a behavior similar to that we have already seen on the right side of the funnel ($Z_1 \to Z_2 \to \cdots \to Z_5$; see Fig. 2) extends to larger groups as b increases.

We have investigated these predictions by doing scans in κ for $N = 10$ (and, in some cases $N = 30$) at $b = 5$, 10, 50 and 200. We find that the HMC algorithm mostly performs well even at these very weak couplings. We did have to reduce the step-size as b increases, such that N_{MD}/acceptance increases roughly like $\sqrt{b}$. We also find that, for $b = 200$, thermalization for each new value of κ sometimes takes longer than our allotted 450 trajectories. On the other hand, the number of CG iterations gradually decreases with increasing b. We also note that run histories of observables show no indication of correlation times that are close to the number of trajectories we were using for measurements (7500).

Results for the plaquette are collected in Fig. 15. The general shape of each curve is similar to those at $b = 1$ (see Fig. 3) but the jump at the putative κ_c falls rapidly with increasing b. This is qualitatively consistent

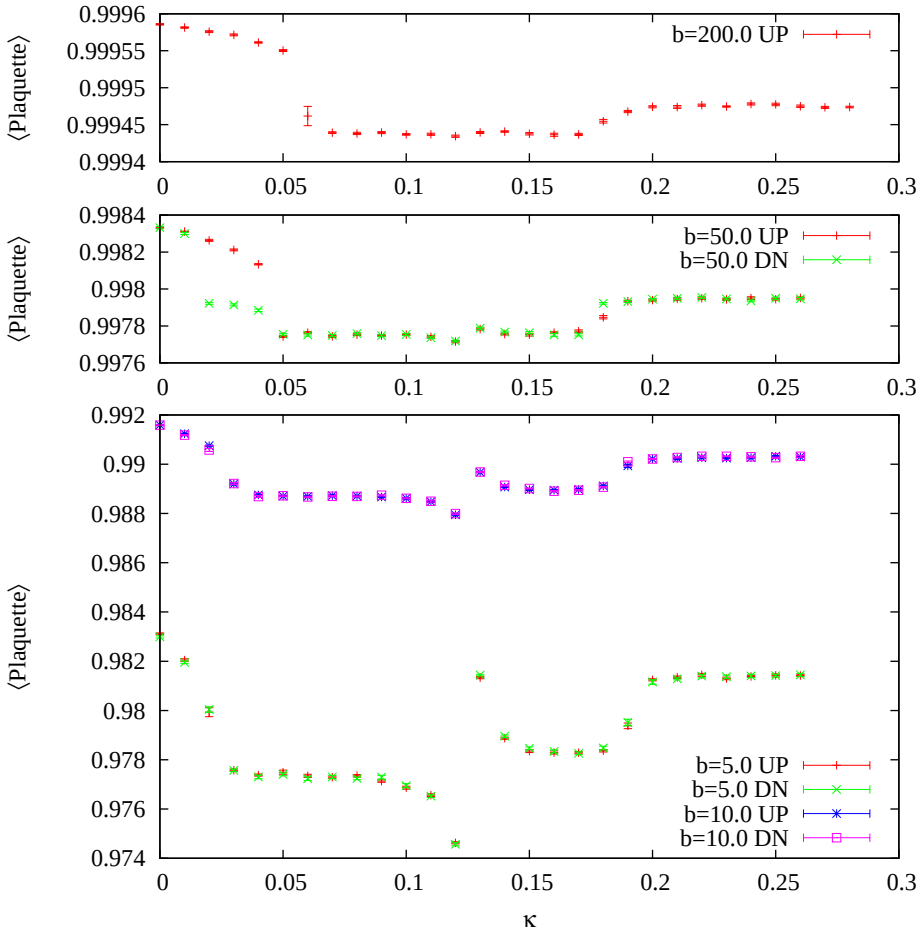

FIG. 15. The average plaquette in scans at extremely high b for $N = 10$. Note the highly compressed vertical scale at large b.

with the expectations from chiral perturbation theory if this is the first-order scenario of Ref. [20].

To verify the hypothesis of Ref. [11] that $am_f = 1/2\kappa_f - 1/2\kappa_c \propto b^{-1/4}$ we analyze the lower edge of the funnel as a function of b. It would obviously be advantageous to repeat the analysis of Sec. IV D for all values of b; unfortunately this is numerically too demanding. We do, however, have estimates of κ_f at $N = 10$ and 30 for a wide range of b. These are shown in Fig. 16. We find that it is harder to determine κ_f for b away from unity. For smaller values, e.g. $b \approx 0.35$, the transition becomes smoother. For much larger values, there is significant hysteresis (as seen in the middle panel of Fig. 15). The net result is that the errors in κ_f are much larger than those at $b = 1$.

Figure 16 also shows fits to $am_f = c\, b^{-1/4}$, with κ_c set to 0.125 for all values of b for simplicity. The fit at $N = 10$ is good, while that at $N = 30$ is poorer. Better fits at $N = 30$ can be obtained using estimates for the actual value of κ_c at each b, but these estimates have sufficient uncertainty that the resulting errors in m_f are substantially increased, so that the agreement with the theoretical form is less significant. Overall we conclude that our results are consistent with the predicted dependence on b.

The figure also indicates that the narrowing of the funnel as N increases holds for all values of b. We do not attempt to extrapolate to $N = \infty$ from $N = 10$ and 30, as our experience with $b = 1$ indicates that $N = 10$ is not in the asymptotic $1/N$ region. However, given that we do find a finite width when $N \to \infty$ at $b = 1$, the observation of mild dependence on b suggests that the funnel will remain of finite width also at other values of b.

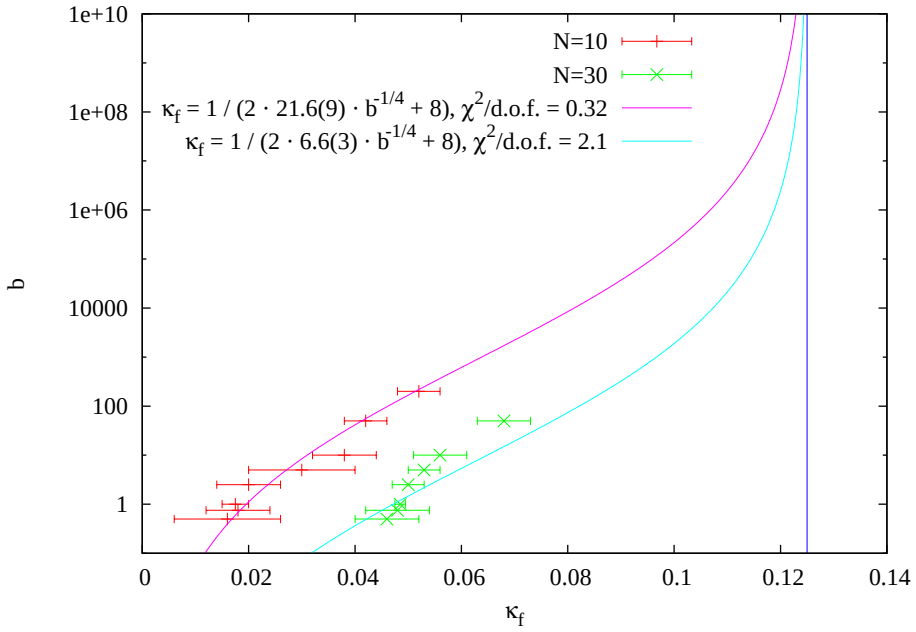

FIG. 16. The dependence of κ_f on b for $N = 10$ and 30. The vertical (blue) line marks $\kappa_c(b = \infty) = 1/8$. The fit functions are discussed in Sec. IV F.

V. MEASUREMENTS INSIDE THE "FUNNEL"

In this section we make a detailed study of the funnel region in which reduction appears to hold using results from $N = 10 - 53$. We consider in turn the spectrum of the single-site Wilson operator D_W, the spectrum of Q^2, and, finally, attempt to extract a physical observable—the heavy-quark potential—from large Wilson loops.

A. Spectrum of D_W

One way of viewing the equivalence of single-site and large-volume theories is that the space-time volume is being packaged inside the gauge matrices. It is thus useful to introduce an effective size, $L_{\rm eff}$, and corresponding effective volume, $L^4_{\rm eff}$, and study their scaling with N. What we mean by $L_{\rm eff}$ is that the single-site theory leads to the same physical results as the theory on an $L^4_{\rm eff}$ volume with $N_{\rm eff}$ colors, up to corrections suppressed by powers of $1/N_{\rm eff}$. Clearly there is a trade-off between increasing $L_{\rm eff}$ and increasing $N_{\rm eff}$. Here we take the approach of holding $N_{\rm eff}$ fixed, but large enough that $1/N_{\rm eff}$ corrections to quantities of interest are small, and then asking how $L_{\rm eff}$ scales with N.

Within this framework, the most conservative possibility is provided by orbifold-based demonstration of volume independence [7]. This demonstration also provides an explicit example of the packaging of the volume into the gauge matrices: the $N \times N$ link matrices are partitioned into blocks of size $N_{\rm eff} \times N_{\rm eff}$, with $N_{\rm eff} = N/L^4_{\rm eff}$, only $L^4_{\rm eff}$ of which are non-zero, and the resultant orbifolded theory is an $SU(N_{\rm eff})$ gauge theory on an $L^4_{\rm eff}$ lattice. Equivalence is demonstrated by holding $L_{\rm eff}$ fixed, and taking N, and thus also $N_{\rm eff}$, to infinity. Instead, using the approach espoused above, if we hold $N_{\rm eff}$ fixed, then increasing N leads to $L_{\rm eff} \propto N^{1/4}$.

A less conservative possibility is obtained, following Refs. [33, 34], by assuming that all entries in the link matrices are used in the packaging of the large volume theory (not just 1 out of every $L^4_{\rm eff}$ as in the orbifold construction). This leads to $L^4_{\rm eff} \sim N^2$ or $L_{\rm eff} \propto N^{1/2}$. There is also a more optimistic possibility, $L_{\rm eff} \propto N$, which is motivated in the Appendix.

The spectrum of the fermion matrix, D_W, can help distinguish these possibilities, as well as give insight into the nature of corrections to the large-N limit. We expect, if reduction holds, that the spectrum should resemble that of a large-volume four-dimensional theory on an $L_{\rm eff}^4$ lattice. In particular, for weak couplings, $b \gtrsim 1$, the spectrum should have the familiar five "fingers" which reach down to the real axis. The number of fingers is a direct indicator of the dimensionality (there are $d+1$ in d dimensions), and the distance of the eigenvalues in the fingers from the real axis should scale as $1/L_{\rm eff}$. These points are discussed in more detail in the Appendix.

We now show some representative results for the spectrum of $D_W(m_0 = 0)$ from our simulations. The operator in the determinant is

$$D_W(m_0) = 2\kappa \left[4D_W(0) + \frac{1}{2\kappa} - 4 \right] = \frac{1}{4+m_0} \left[4D_W(0) + m_0 \right] , \tag{5.1}$$

so that eigenvalues of $4D_W(0)$ close to $\lambda = -m_0 = 4 - 1/2\kappa$ are suppressed. Since the spectrum is bounded, $0 \leq {\rm Re}\lambda \leq 8$, the determinant suppression is important only for $\kappa > 1/8$. We also note that, unlike on a lattice with an even number of sites in each direction, the spectrum is not symmetric under reflection about the ${\rm Re}\lambda = 4$ axis, Thus the first (the leftmost) and fifth fingers are not related by symmetry, and neither are the second and fourth. If such a symmetry holds approximately, it indicates the presence of reduction.

In Fig. 17 we show how the spectrum changes as we vary κ at fixed $b = 1.0$ and $N = 16$. At $\kappa = 0.01$, where we are in the Z_1 phase (see Figs. 3 and 5), we see one main finger and a small indication of a second. This is consistent with the eigenvalues forming a single clump, so that the momenta, given by eigenvalue differences, are all small. At $\kappa = 0.03$ we have moved into the Z_2 phase, with two clumps of eigenvalues. We see that this allows the spectrum to spread into all five fingers, because eigenvalue differences can now range up to π. The details of the spectrum differ from those of a large-volume free fermion, however, in particular having a low density of points in the central three fingers and a "rectangular" shaped envelope. Nevertheless, it is clear that one must interpret the spectrum with care—the presence of five fingers alone does not imply that reduction holds.

The next value, $\kappa = 0.12$, is well inside the funnel, and we see a distribution which is qualitatively similar to that of a free fermion, with a rounded top and five fingers. These features are present for all $\kappa < \kappa_c$ inside the funnel. Particularly noteworthy is the presence of the comet-shaped clump of eigenvalues near the origin. We find that there are exactly $4(N-1)$ eigenvalues per configuration in this clump. We thus interpret them as would-be zero modes, i.e. eigenvalues that would be zero if $b \to \infty$. These modes are dropped in weak coupling calculations, both because they do not impact the dynamics (as they do not depend on the θ_μ^a) and because they form only an $O(1/N)$ fraction of the total number of modes. The spectrum indicates, however, that they could have an important impact on the long-distance dynamics which might overcome their relative paucity. We recall that for a large-volume Wilson operator it is the small eigenvalues which determine long-distance behavior such as chiral symmetry breaking. For very large N we expect small eigenvalues to come dominantly from the first finger, which should approach the real axis. What we see from the figure is that $N = 16$ is quite far from this limit. Thus we conclude that the would-be zero modes are a potential source of the $1/N$ corrections observed above in the plaquette and other quantities, and that their contribution could be sizable (given how far the "true" low-energy modes in the first finger are from the real axis).

The spectrum within the funnel but just above the transition is illustrated by the result for $\kappa = 0.14$. Eigenvalues near ${\rm Re}\,\lambda = 0.43$ are suppressed by the determinant. The would-be zero modes cluster to the left of this excluded point, while the first finger now approaches closer to the real axis. The latter feature indicates that the funnel-region above the transition is more continuum-like, which is consistent with its larger average plaquette. On the other hand, the spectrum as a whole is less symmetric about the ${\rm Re}\lambda = 4$ line than that below the transition.

Moving to $\kappa = 0.17$, which is still inside the funnel, the would-be zero modes have spread out again (perhaps because the excluded point has now moved to $\lambda = 1.06$), while the first finger has become longer and denser. The second finger, however, has almost disappeared.

Finally, at $\kappa = 0.24$ we are in the Z_3 phase. This is reflected by the spectrum breaking into three distinct regions (only two being visible since the third has negative imaginary part), resulting from eigenvalue differences distributed around 0 and $\pm 2\pi/3$.

We have done similar scans at lower b, but the results are less illuminating, because the bulk of the spectrum

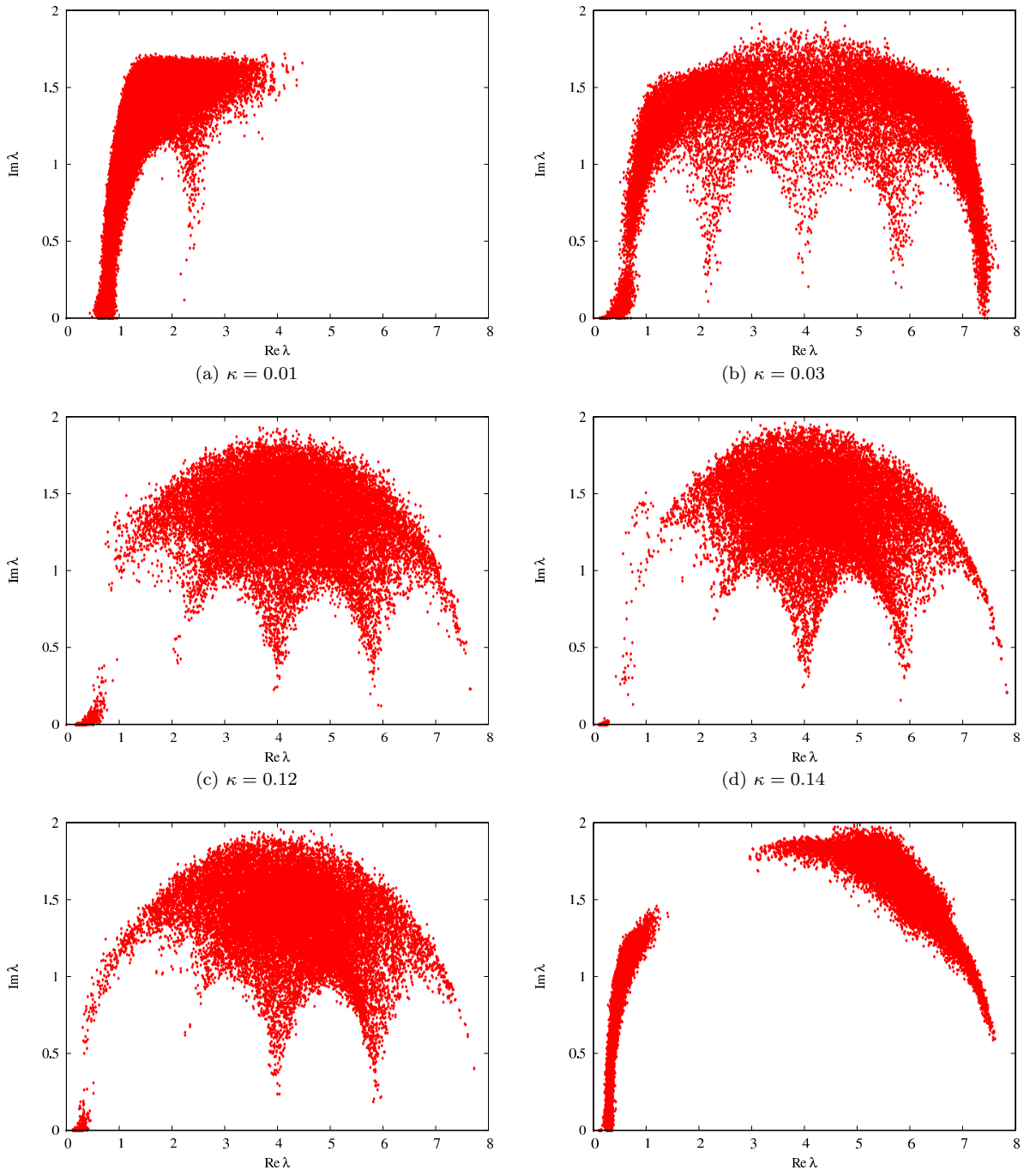

(a) $\kappa = 0.01$ (b) $\kappa = 0.03$

(c) $\kappa = 0.12$ (d) $\kappa = 0.14$

(e) $\kappa = 0.17$ (f) $\kappa = 0.24$

FIG. 17. Spectrum of $4D_W(m_0)$ from simulations at $b = 1.0$ and $N = 30$ at $\kappa = 0.01$, 0.03, 0.12, 0.14, 0.17 and 0.24. Only eigenvalues with positive imaginary part are shown.

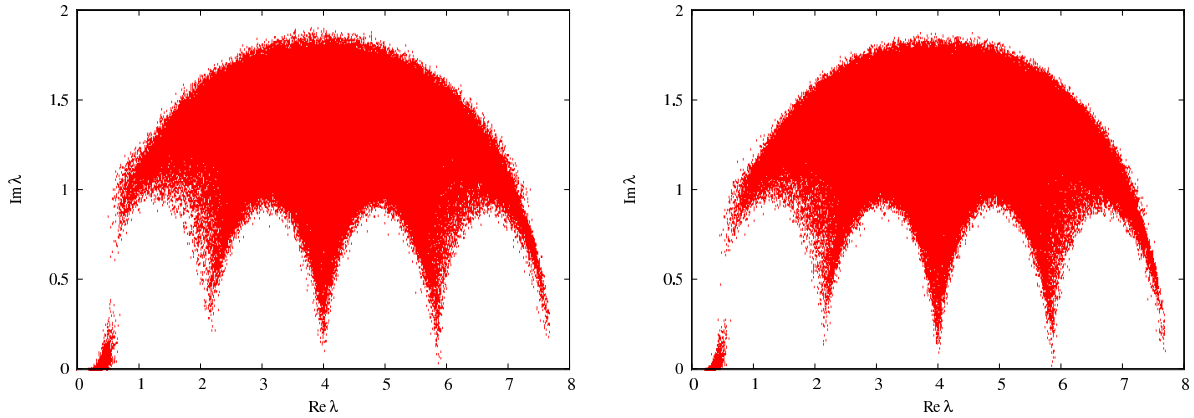

(a) $N = 37$, 300 configs (b) $N = 53$, 150 configs

FIG. 18. Spectrum of $4D_W(m_0)$ at $b = 1.0$ and $\kappa = 0.12$, for $N = 37$ and 53. Note that since $(53/37)^2 \approx 2$ the number of points is approximately the same in both plots.

moves closer to the real axis, such that, at $b = 0.35$, one cannot see any fingers. A better approach is to use the spectrum of Q^2, as described in the following subsection.

We have also studied the N dependence of the spectrum at $b = 1$ and $\kappa = 0.12$. Results from $N = 37$ and 53 are shown in Fig. 18, and can be compared to the $N = 16$ results in Fig. 17(c). The spectra at $N = 37$ and 53 differ very little. The main changes are that the size of the clump of would-be zero-modes decrease as N increases, and that the tip of the first and fifth fingers move down slightly. The tips of the other fingers, however, barely move. Compared to $N = 16$, on the other hand, the fingers are somewhat more extended.

We draw several conclusions from these results. First, the qualitative agreement of the spectrum within the funnel with that from a large volume four-dimensional theory supports our conclusion that reduction holds therein. Second, the $L_{\rm eff} \approx N^{1/4}$, crystalline distribution of eigenvalues described in the Appendix is disfavored, since, for our values of N, it would not lead to the presence of fingers, and thus differ from our results.[13] Third, our results are also inconsistent with the $L_{\rm eff} \approx N$ model, since the fingertips do not approach the real axis as fast as the expected $1/N$. Fourth, the would-be zero-modes are a possible source of $O(1/N)$ corrections. And, finally, these zero-modes may make an important contribution to dynamics, thus enhancing the $1/N$ corrections (again, provided that these $1/N$ corrections are not exactly canceled by $1/N$ corrections from the $4(N^2 - N)$ modes in the bulk of the eigenvalue distribution).

We have also calculated the spectrum of the Dirac operator in the fundamental representation. This gives information directly about the link eigenvalues, rather than their differences. The results confirm our understanding of the phase diagram and eigenvalue distributions explained above, but are not shown for the sake of brevity.

B. Spectrum of Q^2

An alternative view is provided by the spectrum of the squared hermitian Wilson-Dirac operator, $Q^2 = D_W(m_0)D_W(m_0)^\dagger$. Its eigenvalues, λ_{Q^2}, are real and positive. In the continuum limit, the spectrum has a gap, turning on at $\lambda_{Q^2} = (am_{\rm phys})^2$. Away from the continuum limit, the turn-on is smoothed, but still begins approximately at the square of physical bare quark mass [37]. For small enough quark masses, and if there is spontaneous chiral symmetry breaking, the spectrum above the gap is approximately constant, with a value proportional to the condensate. Thus the spectrum can teach us about the size of the quark mass and

[13] We have studied this further by calculating the spectrum on a 2^4 lattice with $N = 3$, corresponding to a "partial crystallization" of a single-site $N = 48$ theory. This spectrum also has no fingers.

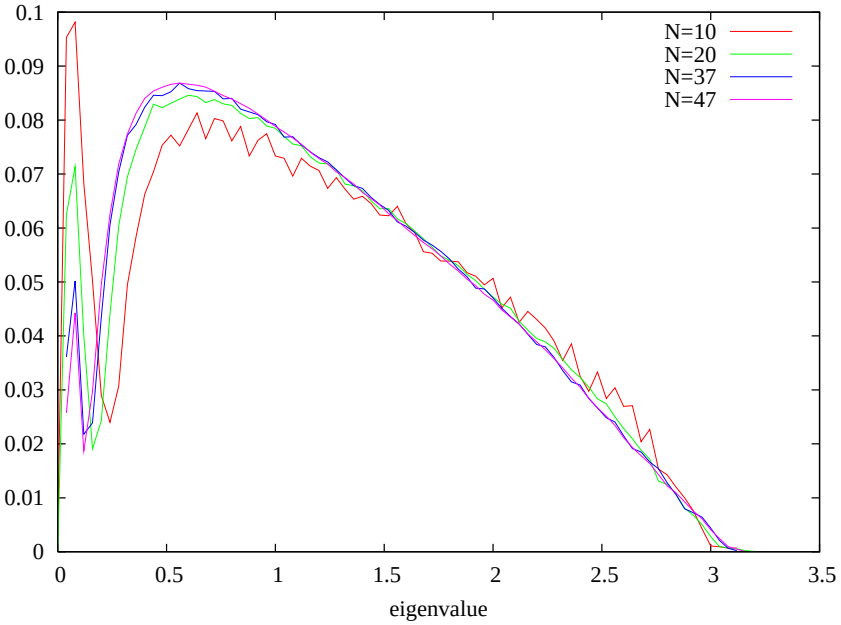

FIG. 19. Spectrum of Q^2 at $b = 0.35$ and $\kappa = 0.12$, for $N = 10$, 20, 37 and 47, using 150, 150, 20 and 60 configurations, respectively. The vertical scale is arbitrary, but the relative scales for different N are chosen so that the area under each spectrum is the same. Errors are not shown, but can be estimated from the kinks in the spectra.

about long-distance physics (assuming reduction holds). The information is also contained in the spectrum of $D_W(0)$, but for $b < 1$, when the fingers are obscured, is hard to extract. Thus we have used the spectrum of Q^2 mainly for $b = 0.35$, which, we recall, is a bare coupling close to those used in typical large-volume simulations.

Results for $b = 0.35$, $\kappa = 0.12$ and $N = 10 - 47$ are shown in Fig. 19. (Results at $N = 53$ are very similar to those at $N = 47$ but have lower statistics and are thus not shown.) The spectra are normalized to have the same integral, so that the large N limit can be taken. The peak at small eigenvalues has the correct area to contain just the would-be zero modes, so that its area drops as $1/N$ in the normalized spectrum. It will disappear entirely when $N \to \infty$. The bulk of the eigenvalues form a "hump" which at the upper end ($\lambda_{Q^2} \gtrsim 1.5$) is approximately independent of N, while at the lower end depends on N. The form of the hump at $N = 47$ should give a good approximation to the form at $N = \infty$ because the small-eigenvalue peak has little area left to "redistribute" to the hump. A crude extrapolation of the leading edge of the hump at $N = 47$ suggests that the gap at $N = \infty$ will be at $\lambda_{Q^2} \approx 0.1$. This corresponds to a quark mass of $am_{\rm phys} \approx 0.3$, modulo the unknown renormalization factor, which, however, we expect to be of $O(1)$. This is the only "measurement" of the quark mass that we have obtained, and shows that the quark is relatively heavy, not much below $m_{\rm phys} = 1/a$.

These results shed light on the issue of how large N needs to be for reduction to be useful. On the one hand, one can seen that the bulk of the eigenvalues (those in the hump) are close to their large N limit by $N \approx 40$. On the other hand, the would-be zero modes, though making up only an $O(1/N)$ fraction of the total, are the dominant contribution in the low mode region. Which effect is more important is not clear *a priori*—one must calculate physical observables and study their N-dependence.

C. Large Wilson loops

Our ultimate aim in studying the single-site models is to use them to calculate physical quantities in phases where large-N reduction holds. An important quantity that should be accessible in such phases is the heavy-

quark potential. To obtain this we calculate rectangular Wilson loops using the large-N reduction recipe (and also averaging over orientations):

$$W(L_1, L_2) = \frac{1}{12} \sum_{\mu \neq \nu} \left\langle \frac{1}{N} \mathrm{Re\,tr} \left(U_\mu^{L_1} U_\nu^{L_2} U_\mu^{\dagger\, L_1} U_\nu^{\dagger\, L_2} \right) \right\rangle , \tag{5.2}$$

For $N \to \infty$ the result should equal the infinite-volume large-N value. The potential can be obtained as usual from the large L_2 behavior

$$W(L_1, L_2) \stackrel{L_2 \to \infty}{\longrightarrow} c(L_1) e^{-V(L_1) L_2} . \tag{5.3}$$

At large L_1 we expect linear behavior if we are in a confining regime:

$$\frac{dV(L_1)}{dL_1} \stackrel{L_1 \to \infty}{\longrightarrow} \sigma . \tag{5.4}$$

For finite N, reduction will only give useful results for loops whose sizes satisfy $L_j \ll N$, and the key question is how much smaller than N do the L_j need to be. Another important question is whether it suffices to calculate Wilson loops using unsmeared links, i.e. whether the statistical errors will overwhelm any signal of interest. State-of-the-art calculations in large volumes use smearing, as well as other noise reduction techniques.

In our earlier study of the $N_f = 1$ model [8], in which $N \lesssim 13$, we did not find a useful "window" as a function of the L_j. For fixed L_1, for example, the dependence on L_2 was a rapid drop for a few points followed by a slow rise. The drop was not extensive enough to determine the potential from the coefficient of the exponential. Here we have results extending up to $N = 53$, and thus expect that the situation will be substantially better.

In Fig. 20 we show results for $1 \times L$ loops for a range of values of N on a log-linear scale. For each value of N we find an approximately exponential decrease followed by slow, roughly linear increase. The latter we interpret as a finite N effect, since it begins at larger values of L as N increases. The good news from this plot is that we see convergence to the expected exponential drop-off as N increases. For example, at $L = 6$ the $N = 37$ point has "peeled-off" the linear envelope, but the $N = 47$ and 53 points are in good agreement. This is large-N reduction in action. The bad news is that the maximum value of L at which convergence occurs, L_{max}, grows only slowly with N. This is not unexpected: we are trying to extract an exponentially falling contribution to a quantity which has finite N corrections. To estimate the size of these corrections, one can look at the the minimum value of the loop as a function of L, which we find falls as approximately $1/N$. Thus L_{max} grows only logarithmically with N, which presents a significant numerical challenge.

Despite this challenge, we see from the figure that we can extract a value for the slope at small L with reasonably small errors. This gives $-V(1)$, the potential at unit separation. To extract σ, we need the potential at larger separations. We show in Fig. 21 the results for $5 \times L$ loops. The overall pattern is similar to those for $1 \times L$ loops, but the convergence in N of the falling parts of the curves is much poorer. Only results for $L \leq 2$ appear converged. Thus we cannot extract $V(5)$ with any reliability. It is of course not a surprise that difficulty of determining $V(L)$ increases with L, since the signal falls off more quickly while the $1/N$ background is little changed.

Concerning statistical errors, we see from both of these plots that 20 configurations is sufficient to pull out the rapidly falling part of the curves. The problem is not the statistical errors, but rather the $1/N$ corrections.

We have carried out a similar investigation at other points in the funnel. We find that as b increases, the slope of the initial fall-off decreases. If we move to the other side of the transition (where the average plaquette is closer to unity) we find that the slope decreases further, and also that the large-L approximately linear rise changes to an almost L-independent behavior.

It would clearly be of interest to gain some understanding of the large L behavior of the Wilson loops. The only analytic approach that we are aware of that can shed some light on the issue is to calculate the loops in strong coupling. In the $b = 0$ limit, and ignoring the fermion determinant, the gauge links are distributed

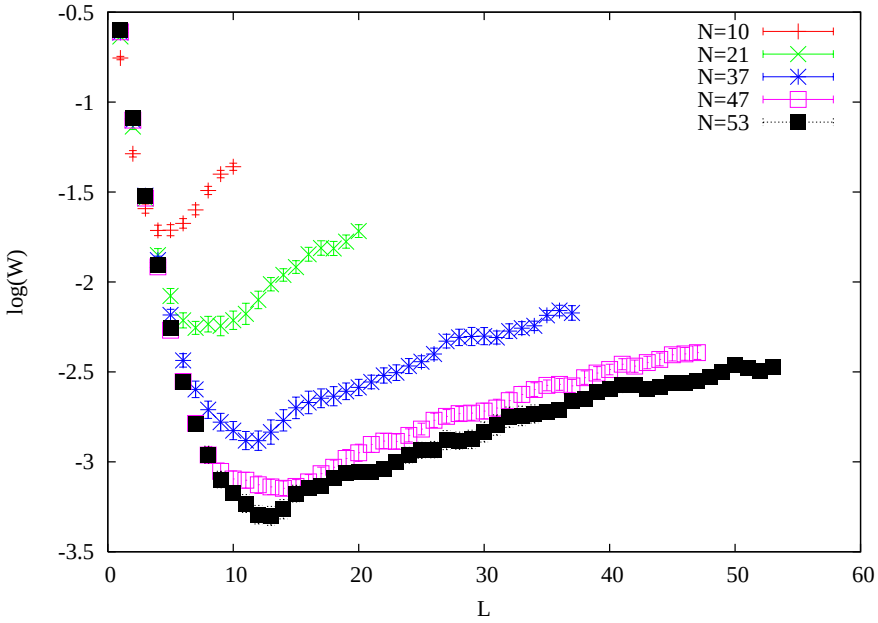

FIG. 20. Log-linear plot of $1 \times L$ Wilson loop versus L for $L \leq N$. Results are from $b = 0.35$, $\kappa = 0.12$ and for $N = 10$, 21, 37, 47 and 53, using 20 configurations except for $N = 10$ where we use 150.

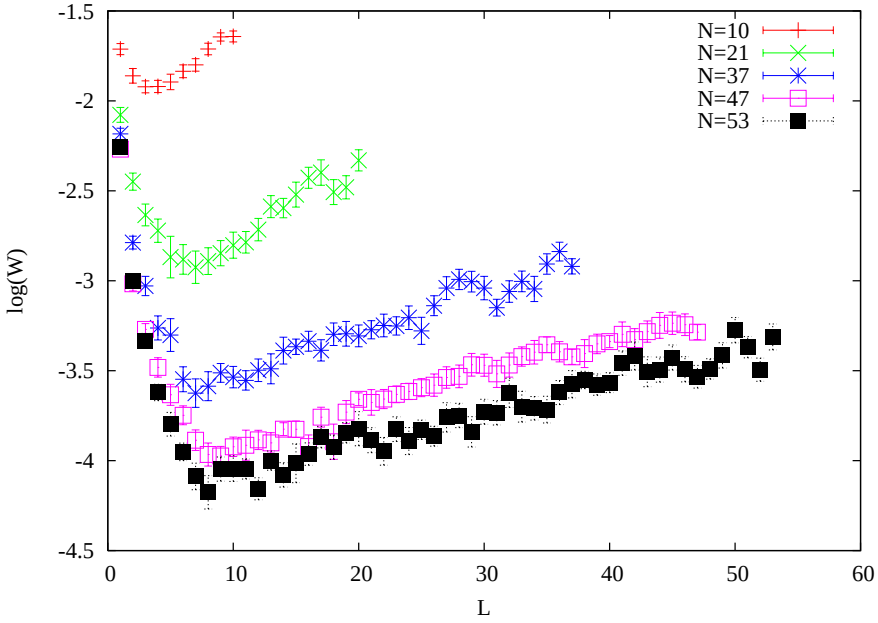

FIG. 21. As for Fig. 20 except for $5 \times L$ loops.

according to the Haar measure, and one can show that[14]

$$W(L_1, L_2) \stackrel{b,\kappa\to 0}{\longrightarrow} \frac{1}{N^2-1}\left(L_1 + L_2 - 1 - L_1 L_2/N^2\right) \qquad \text{for } 0 < L_1, L_2 \le N\,. \tag{5.5}$$

For $L_j \sim O(1)$, the contribution is of $O(1/N^2)$, rising to of $O(1/N)$ when at least one of the L_j is of $O(N)$. This shows how the correlations can lead to an increasing result as one of the L_j is increased, which is qualitatively in agreement with the results of Figs. 20 and 21. Quantitatively, this model does not, however, reproduce our data at $b \sim 1$. For example, we would expect that $W_{\min} \sim 1/N^2$ in the model, but we find instead an approximate $1/N$ dependence.

VI. DISCUSSION AND OUTLOOK

We have presented a detailed study of the single-site version of large-N QCD with two flavors of adjoint Dirac fermions—the so-called Adjoint Eguchi-Kawai (AEK) model—discretized using Wilson's gauge and fermion actions. This seemingly simple model turns out to have a rich phase structure, as shown in Fig. 2, some aspects of which can be understood semi-quantitatively [11]. Our most important result is that we find, for N up to 53, and for b up to 200, a broad funnel in the (κ, b) plane in which the Z_N^4 center symmetry is unbroken. This region encompasses both light ($\kappa \to \kappa_c$) and heavy ($m \sim 1/a$) quarks. While the funnel narrows as $N \to \infty$, we present strong evidence that it remains of finite width in this limit. If so, then the single-site theory, when simulated within the funnel, is equivalent to the corresponding large-volume theory, up to corrections, suppressed by powers of $1/N$, which can be made arbitrarily small. Thus one can use the single-site model to study the large-N version of the minimal walking technicolor (MWT) model discussed in the Introduction.

In particular, the phase structure we find *within the funnel* should be identical to that of the large-N MWT model. We find a first-order transition, with a discontinuity in the plaquette (and other variables), for values of b at least up to $b \approx 1$ (see Fig. 15). This is in contrast to the results of direct large-volume simulations of the $N = 2$ two-adjoint model, which find that the transition changes from first-order at strong coupling to second-order at weak coupling, with the transition occurring at $b \approx 0.25$ [25, 26]. The quark mass vanishes along the second-order portion of the transition line, and it is in part by studying the non-perturbative β-function along this segment of the line that evidence has been found for an infrared fixed point. Further evidence that the $N = 2$ theory is conformal in the infrared comes from studies of the spectrum and other quantities as one approaches the second-order line (as summarized in Refs. [15, 16]).

The most straightforward interpretation of our phase diagram is that the theory is confining in the infrared, with chiral symmetry spontaneously broken, and that the first-order transition is an example of the first-order scenario of Ref. [20] in which the chiral condensate flips sign. The transition is a result of competition in the effective potential for the condensate between terms proportional to the fermion mass m and discretization errors of size $a^2\Lambda^3$. Here Λ is the confinement scale, and it is essential for this picture that such a scale is present. The analysis predicts that the discontinuity should drop rapidly as b increases, which is qualitatively consistent with our numerical results.

An alternative interpretation is that the transition is a "bulk" transition, which happens to extend to large b, but at some finite $b_c > 1$ becomes a second-order line. This would be an extreme version of what happens for the $N = 2$ theory, where the bulk transition extends to $b \approx 0.25$. In this picture discretization errors do not allow one to approach the massless theory, except for extremely weak coupling, so that one cannot determine the infrared properties of the massless theory.[15] We view this as an unlikely possibility, since bulk transitions occur generically at strong coupling.

Whatever the interpretation, it is striking that there is such a large difference in the phase diagrams of the $N = 2$ and $N = \infty$ theories. On the one hand, such a difference is in conflict with the models of Ref. [39]

[14] Note that these loops all vanish in infinite volume at strong coupling. One obtains a non-zero result on a single-site lattice because the U_μ and $U_\mu^\dagger$ terms in the loop are correlated.

[15] We note that there is no problem in principle with using single-site models to study theories in the conformal window, as stressed in Ref. [12].

for the position of the conformal window, which give N-independent predictions. On the other, we note that the beta-function (for the coupling b) does depends on N, starting at four-loop order. The situation clearly warrants further study.

Another result of our work is that we find strong evidence for $1/N$ corrections when extrapolating the average plaquette to $N = \infty$. This is consistent with perturbation theory, which predicts $1/N$ effects at one-loop order for a single site theory, in contrast to the $1/N^2$ corrections that one finds in infinite volume. Based on our study of the spectrum of D_W, the Wilson-Dirac operator, we suggest that another source of $1/N$ corrections may be the contributions of the $4(N-1)$ modes of D_W that become zero-modes when $b \to \infty$. One caveat with our suggestion for the source of the $1/N$ behavior is that the contribution of the would-be zero-modes can be canceled by those from other modes. This happens in infinite-volume perturbation theory (as in the results for the first two terms of the β-function mentioned above) and also at strong coupling [as in the result for Wilson-loops of fixed size at strong coupling, eq. (5.2)]. We also note that the presence of significant $1/N$ dependence in the plaquette may be related to the apparent difference between the phase diagrams of the $N = 2$ and $N = \infty$ theories.

If, as our results suggest, reduction holds within the funnel, then a lattice theory with multiple sites is being packaged inside the four link matrices and single-site fermion fields. One can think, approximately, of an effective lattice size, $L_{\rm eff}$. It is important for practical applications to determine how $L_{\rm eff}$ grows with N. Our results for the spectrum of D_W (which, within the funnel, looks qualitatively similar to that on a large volume, cf. Fig. 18) suggest that neither the most pessimistic ($L_{\rm eff} \propto N^{1/4}$) nor the most optimistic ($L_{\rm eff} \propto N$) possibilities hold. Let us assume, then, that $L_{\rm eff} \propto N^{1/2}$—an intermediate possibility motivated in Sec. V A—and consider the question of whether, if one wants to determine the large-N properties of a theory, it is computationally advantageous to use a single-site theory or one on a large volume, L^4. In the former case, we have found from our simulations that, for fixed b and κ, and with κ near to κ_c,

$$\mathrm{CPU(1\text{-}site)} \propto N^{4.5} \propto L_{\rm eff}^5 N^2 \,, \tag{6.1}$$

where in the final expression we have used $L_{\rm eff} \propto N^{1/2}$. For the large volume theory we expect (for fixed lattice spacing and fermion mass)

$$\mathrm{CPU}(L^4) \propto L^5 N^3 \,, \tag{6.2}$$

where the L^5 is the standard hybrid Monte-Carlo volume scaling [40], while N^3 is the operation count for the core operation of $N \times N$ matrix multiplies. This comparison suggests that the single-site approach could be computationally advantageous. While there are many caveats to this conclusion (e.g. the single-site scaling form is based on simulations for a finite range of N, and the scaling of $L_{\rm eff}$ with N is not established), we take it as motivation to further pursue studies of reduced models.

One aspect of such studies is calculating physical quantities such as the string tension and particle masses. We have taken a first step in this direction by calculating large Wilson loops and attempting to extract the heavy-quark potential. We find that we can do so for small separations (roughly out to 3 lattice spacings for $b = 0.35$) but not beyond. The difficulty arises because the signal must be determined from an exponential decay as a function of the loop size, while the corrections to reduction lead to a "background" of $O(1/N)$ which is approximately independent of loop size. As the coefficient of the decay—the potential, or more generally a hadron mass—increases, one has to go to ever higher values of N. This problem should be less serious, however, for light particles, such as one expects to find as κ approaches κ_c. Indeed, calculating the pion mass would allow an important cross-check on our preferred interpretation that the system is confining, and chiral-symmetry breaking, in the infrared.

One can also use the $N_f = 2$ AEK model away from the critical line as a single-site model whose long distance physics is that of the pure gauge theory. In other words, heavy adjoint fermions resolve the problems of the original Eguchi-Kawai model. The same holds true for the $N_f = 1$ theory [8, 11].

To address the unresolved issues described above, one will need either to work at larger N or move to models with more than one site. The latter option seems most practical, and also has the advantage of being simpler to parallelize. First steps in this direction have been taken in Ref. [19]. It may also be advantageous to use twisted boundary conditions, as has been done for the $N_f = 1$ theory in Ref. [11], since these appear to reduce the power of the corrections from $1/N$ to $1/N^2$. One can also consider using improved gauge and fermion actions, since these are known to clarify the infrared behavior in large-volume simulations [27].

ACKNOWLEDGMENTS

We thank Mithat Ünsal for discussions and Adi Armoni, Simon Catterall, Ari Hietanen, Mithat Ünsal and the referee for comments on the manuscript. This work was supported in part by the U.S. DOE Grant No. DE-FG02-96ER40956, and by Foundation for Polish Science MPD Programme co-financed by the European Regional Development Fund, agreement no. MPD/2009/6. MK is grateful to the University of Washington for hospitality. Most of the numerical simulations were done using the Shiva computing cluster at the Faculty of Physics, Astronomy and Applied Computer Science, Jagiellonian University, Cracow.

Appendix A: Models for eigenvalues of D_W

In this appendix we describe various possible behaviors of the link eigenvalues and their implications for the eigenvalues of D_W. These models guide the interpretation of the results presented in Sec. V A for the spectrum of D_W.

We consider the extreme weak coupling limit, $b \gg 1$, in which we must choose links that maximize $S_{\rm gauge}$. This is achieved by links which can simultaneously diagonalized by a gauge transformation, i.e. for which one can have

$$U_\mu = \mathrm{diag}\left(e^{i\theta_\mu^1}, e^{i\theta_\mu^2}, \dots e^{i\theta_\mu^N}\right) \quad \forall \mu\,. \tag{A1}$$

What is needed for D_W is the link in the adjoint representation [see Eq. (2.4)]. It is convenient to add a singlet and consider the link in the reducible $N \otimes \overline{N}$ representation. In this case, it has composite indices, $A = (a_1, a_2)$, with $a_j = 1, N$, and is also diagonal:

$$\left(U_\mu^{N\otimes\overline{N}}\right)_{AB} = \left(U_\mu\right)_{a_1 b_1} \left(U_\mu\right)_{a_2 b_2} \quad \Rightarrow \quad U_\mu^{N\otimes\overline{N}} = \mathrm{diag}\left(\dots, e^{i(\theta_\mu^{a_1} - \theta_\mu^{a_2})}, \dots\right)\,. \tag{A2}$$

Inserting this into the massless Wilson-Dirac operator, one finds[16]

$$4D_W(m_0 = 0) = \mathrm{diag}\left(\dots, \left\{(4 - \sum_\mu \cos\theta_\mu^{a_1 a_2}) + i\sum_\mu \gamma_\mu \sin\theta_\mu^{a_1 a_2}\right\}, \dots\right)\,, \tag{A3}$$

where we are using the abbreviation

$$\theta_\mu^{a_1 a_2} = \theta_\mu^{a_1} - \theta_\mu^{a_2}\,. \tag{A4}$$

Thus D_W is diagonal in color space, but not in Dirac space. The eigenvalues of $D_W(m_0 = 0)$ are as follows. There are $4N$ zero-modes, occurring when $a_1 = a_2$ so that $\theta_\mu^{a_1 a_2} = 0$. Four of these are from the singlet, which we can now remove, leaving $4(N-1)$ from the adjoint. The remaining $4N(N-1)$ are each doubly degenerate (due to charge conjugation symmetry) and come in complex conjugate pairs (due to γ_5-hermiticity), and have values

$$\lambda_{a_1 a_2} = (4 - \sum_\mu \cos\theta_\mu^{a_1 a_2}) \pm i\sqrt{\sum_\mu \sin^2\theta_\mu^{a_1 a_2}}\,, \quad (a_1 \neq a_2)\,. \tag{A5}$$

The form of D_W in Eq. (A3) is exactly that of a four-dimensional free massless Wilson-Dirac fermion, with the momenta in lattice units ap_μ replaced by $\theta_\mu^{a_1 a_2}$. This is the standard way in which the large volume appears in the weak coupling limit, i.e. link eigenvalue differences become momenta [2]. If these eigenvalue differences are distributed such that the resulting "momenta" lie uniformly throughout a four-dimensional

[16] We multiply by $4 = 1/[2\kappa_c(g^2 = 0)]$ in order that (in large volume) the operator becomes the Dirac operator with standard normalization in the naive continuum limit. This undoes the standard renormalization of the fermion fields by $\sqrt{2\kappa}$ that is used to write D_W in the form of Eq. (2.4).

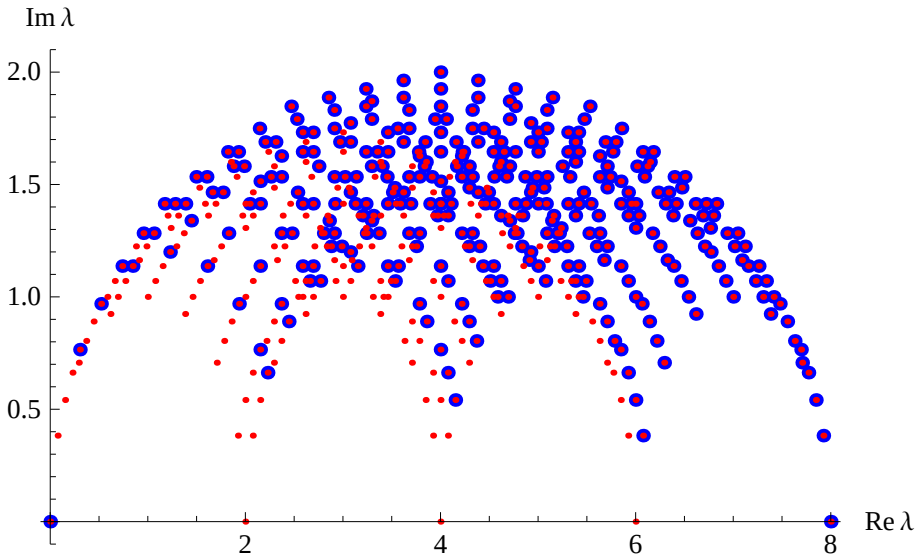

FIG. 22. Spectrum of $4D_W(0)$ in the model given by Eq. (A6) for $N = 16$ and with $O(N^2)$ configurations (large [blue] dots) compared to the spectrum of the free Wilson-Dirac operator on a 16^4 lattice (small [red] dots). Only eigenvalues with positive imaginary part are shown; the spectra are symmetric under reflection in the Reλ axis.

Brillouin zone, then the single-site D_W will approximate that of large-volume four-dimensional theory. The resulting spectrum has the five fingers mentioned above, whose "tips" occur when all four ap_μ equal 0 or π. The tips are distinguished by the number of ap_μ which equal 0—either 0, 1, 2, 3 or 4. Alternatively, if the eigenvalues are correlated in some way, then the spectrum will not, in general, have five fingers. There would, for example, be fewer fingers if the effective dimensionality is less than four.[17]

To illustrate these comments we discuss the results from three simple (and somewhat artificial) models for the eigenvalue distributions. In the first, we choose the eigenvalues in each direction to be evenly spaced around the unit circle, but in a randomly permuted order, with the permutation being independent in each direction. This leads to

$$\theta_\mu^{a_1 a_2} = \frac{2\pi}{N}[\sigma_\mu(a_1) - \sigma_\mu(a_2)]\,, \tag{A6}$$

with σ_μ a permutation of $1 - N$. In the eigenvalue-momentum correspondence these are the subset of the momenta available on an N^4 lattice with periodic boundary conditions. The Brillouin zone of such a lattice contains N^4 momenta, which is much larger than the N^2 values of $\theta_\mu^{a_1 a_2}$ produced by a single configuration. We thus assume further that independent configurations lead to independent permutations. Then, with of $O(N^2)$ configurations, one obtains the spectrum shown in Fig. 22 by the large (blue) dots. This is compared in the figure to the full spectrum of a 4-d free Wilson-Dirac operator on an N^4 lattice. One sees the appearance of the desired 5 fingers, but also that some points in the full spectrum are missing. This is due to the fact that $\theta_\mu^{a_1 a_2} = 0$ only if $a_1 = a_2$, in which case $\theta_\mu^{a_1 a_2} = 0$ for all μ. The model thus cannot produce momenta proportional to $(0, 0, 0, n_4)$, $(0, 0, n_3, n_4)$ or $(0, n_2, n_3, n_4)$ (or their permutations). These "missing modes" have the largest impact on the left-most (and thus physical) finger, but become increasingly unimportant as N increases. We note that the distance of the fingertips to the real axis scales as $1/N$.

In this model center symmetry is unbroken, and in particular all traces of open loops, K_n, vanish (unless all four n_μ are integer multiples of N). It gives an example where the effective size is $L_{\rm eff} = N$, in the sense that

[17] Given the weak-coupling form (A5), the spectrum is necessarily confined to lie between the ellipse $(R-4)^2 + (2I)^2 = 16$ and the four circles $(R - R_0)^2 + I^2 = 1$, with $R_0 = 1$, 3, 5, and 7. Here R and I are respectively the real and imaginary parts of the eigenvalues. Thus the distribution is kinematically forced to lie in one of the five fingers once $|I| < 1$. The presence of fingers *per se* is thus not significant, but the number of fingers which are populated is significant.

the fermion operator after averaging over configurations has the same spectrum as a theory with volume N^4. The model is artificial in that eigenvalues do not fall on the "clock" values in unbroken phase, but, as seen above, are spread nearly uniformly. Nevertheless, it indicates how the spectrum of D_W can teach us about the distribution of eigenvalues and the effective dimensionality.

Our second model is a variant of the first in which the eigenvalues still take clock values, but they are fully correlated between the directions. This breaks the Z_N^4 center symmetry down to the "diagonal" Z_N subgroup. More precisely, we assume that $\theta_\mu^a = \theta_\nu^a + (2\pi/N)n_{\nu,\mu}$ for all a, μ and ν, with $n_{\nu,\mu}$ an integer. This leads to

$$\theta_\mu^{a_1 a_2} = \frac{2\pi}{N}[\sigma(a_1) - \sigma(a_2)]\,, \tag{A7}$$

where now there is a single permutation σ for all four directions. This is the type of "locking" found in the quenched EK (QEK) model [29]. It leads to the spectrum of D_W being that of a 1-d free Wilson fermion in a periodic box of length $L_{\rm eff} = N$, scaled up by a factor of 4. In this case the central three fingers are missing.

The third model is inspired by the analysis of Ref. [12], in which it is shown that, at extremely weak coupling, the repulsion between eigenvalues leads to the formation of a four-dimensional crystal if $K = N^{1/4}$ is an integer, and an approximately uniform distribution for other values of N. It is important to note that the analysis of Ref. [12] holds only if the coupling b evaluated at the scale $1/(aL_{\rm eff})$ is much larger than unity. This requires that the lattice coupling, $b(1/a)$, grows logarithmically with N. This is not the standard limit in which reduction holds, in which b is fixed. Indeed, volume independence does not hold in this regime. We can express this realization of eigenvalues as

$$[\theta_1^a, \theta_2^a, \theta_3^a, \theta_4^a] = \frac{2\pi}{K}\left[\mathrm{mod}(a-1,K), \mathrm{mod}(\frac{a-1}{K},K), \mathrm{mod}(\frac{a-1}{K^2},K), \mathrm{mod}(\frac{a-1}{K^3},K)\right]\,, \tag{A8}$$

which breaks the center symmetry down to Z_K^4, but it is argued in Ref. [12] that fluctuations in the eigenvalues can lead to an averaging over the different "crystals" related by Z_N^4 transformations, and thus the restoration of the full symmetry. The momenta $\theta_\mu^{a_1,a_2}$ are the same for all crystals, and lead to a four-dimensional spectrum for D_W.[18] The difference from the first model is that instead of the spectrum being that on a lattice of size $L_{\rm eff} = N$ it is on the much smaller size $L_{\rm eff} = K = N^{1/4}$. This is the same scaling as for the orbifold construction discussed in the main text, and is the most conservative possibility.

For the values of N that we use, one has $L_{\rm eff} < 3$. For such a small lattice, even though it is four-dimensional, the spectrum shows no fingers, i.e. no eigenvalues close to the real axis. Thus if this model of the eigenvalues provides even an approximate description of our data, we would not expect to see fingers.

It is interesting that the above distribution of eigenvalues was first suggested in the context of the space embedding into color space of the QEK model [35], and then analyzed in Ref. [36]. For a further discussion on this point see Ref. [29] where two of us analyzed this eigenvalue distribution within the QEK model (where it is referred to as the 'Brillouin Zone' distribution).

[1] T. Eguchi and H. Kawai, Phys. Rev. Lett. **48**, 1063 (1982).
[2] G. Bhanot, U. M. Heller and H. Neuberger, Phys. Lett. B **113**, 47 (1982).
[3] V. A. Kazakov and A. A. Migdal, Phys. Lett. B **116**, 423 (1982).
[4] M. Okawa, Phys. Rev. Lett. **49**, 353 (1982).
[5] H. Neuberger, Annales Henri Poincare **4**, S147 (2003) [arXiv:hep-th/0212097].
[6] P. Kovtun, M. Ünsal and L. G. Yaffe, JHEP **0507**, 008 (2005) [arXiv:hep-th/0411177].
[7] P. Kovtun, M. Ünsal and L. G. Yaffe, JHEP **0706**, 019 (2007) [arXiv:hep-th/0702021].
[8] B. Bringoltz and S. R. Sharpe, Phys. Rev. D **80**, 065031 (2009) [arXiv:0906.3538 [hep-lat]].
[9] B. Bringoltz, JHEP **1001**, 069 (2010) [arXiv:0911.0352 [hep-lat]].
[10] T. J. Hollowood, J. C. Myers, JHEP **0911**, 008 (2009) [arXiv:0907.3665 [hep-th]].

[18] Note that in this case a single configuration suffices to fill out the spectrum.

[11] T. Azeyanagi, M. Hanada, M. Ünsal and R. Yacoby, Phys. Rev. **D82**, 125013 (2010) [arXiv:1006.0717 [hep-th]].
[12] M. Ünsal, L. G. Yaffe, JHEP **1008**, 030 (2010) [arXiv:1006.2101 [hep-th]].
[13] A. Hietanen, R. Narayanan, JHEP **1001**, 079 (2010) [arXiv:0911.2449 [hep-lat]].
[14] A. Hietanen, R. Narayanan, Phys. Lett. **B698**, 171-174 (2011) [arXiv:1011.2150 [hep-lat]].
[15] K. Rummukainen, AIP Conf. Proc. **1343**, 51 (2011) [arXiv:1101.5875 [hep-lat]].
[16] L. Del Debbio, [arXiv:1102.4066 [hep-lat]].
[17] A. Armoni, M. Shifman and G. Veneziano, Phys. Rev. Lett. **91**, 191601 (2003) [arXiv:hep-th/0307097].
[18] E. Corrigan, P. Ramond, Phys. Lett. **B87**, 73 (1979).
[19] S. Catterall, R. Galvez, M. Ünsal, JHEP **1008**, 010 (2010) [arXiv:1006.2469 [hep-lat]].
[20] S. R. Sharpe and R. L. Singleton, Jr., Phys. Rev. D **58**, 074501 (1998) [arXiv:hep-lat/9804028].
[21] L. Del Debbio, M. T. Frandsen, H. Panagopoulos and F. Sannino, JHEP **0806**, 007 (2008) [arXiv:0802.0891 [hep-lat]].
[22] S. Aoki, Phys. Rev. D **30**, 2653 (1984).
[23] P. H. Damgaard, K. Splittorff, J. J. M. Verbaarschot, Phys. Rev. Lett. **105**, 162002 (2010) [arXiv:1001.2937 [hep-th]].
[24] G. Akemann, P. H. Damgaard, K. Splittorff and J. J. M. Verbaarschot, Phys. Rev. D **83**, 085014 (2011) [arXiv:1012.0752 [hep-lat]].
[25] S. Catterall, J. Giedt, F. Sannino *et al.*, JHEP **0811**, 009 (2008) [arXiv:0807.0792 [hep-lat]].
[26] A. J. Hietanen, J. Rantaharju, K. Rummukainen *et al.*, JHEP **0905**, 025 (2009) [arXiv:0812.1467 [hep-lat]].
[27] T. DeGrand, Y. Shamir and B. Svetitsky, Phys. Rev. D **83**, 074507 (2011) [arXiv:1102.2843 [hep-lat]].
[28] S. Duane, A. D. Kennedy, B. J. Pendleton, D. Roweth, Phys. Lett. **B195**, 216-222 (1987).
[29] B. Bringoltz, S. R. Sharpe, Phys. Rev. **D78**, 034507 (2008) [arXiv:0805.2146 [hep-lat]].
[30] C. Allton, M. Teper, A. Trivini, JHEP **0807**, 021 (2008) [arXiv:0803.1092 [hep-lat]].
[31] W. Bietenholz, J. Nishimura, Y. Susaki and J. Volkholz, JHEP **0610**, 042 (2006) [arXiv:hep-th/0608072];
T. Azeyanagi, M. Hanada, T. Hirata, T. Ishikawa, JHEP **0801**, 025 (2008) [arXiv:0711.1925 [hep-lat]];
M. Teper and H. Vairinhos, Phys. Lett. B **652**, 359 (2007) [arXiv:hep-th/0612097].
[32] J. Kiskis, R. Narayanan, H. Neuberger, Phys. Lett. **B574**, 65-74 (2003) [hep-lat/0308033].
[33] J. Ambjorn, Y. M. Makeenko, J. Nishimura, R. J. Szabo, JHEP **9911**, 029 (1999) [hep-th/9911041].
[34] M. Ünsal, JHEP **0512**, 033 (2005) [hep-th/0409106].
[35] D. J. Gross and Y. Kitazawa, Nucl. Phys. B **206**, 440 (1982).
[36] I. Bars, Based on lectures given at 21st Int. Conf. on High Energy Physics, Paris, France, Jul 26-31, 1982. Published in Trieste Field Theor.Wkshp.1982:168 (QCD161:W614:1982).
[37] L. Giusti, M. Luscher, JHEP **0903**, 013 (2009) [arXiv:0812.3638 [hep-lat]].
[38] A. J. Hietanen, K. Rummukainen, K. Tuominen, Phys. Rev. **D80**, 094504 (2009) [arXiv:0904.0864 [hep-lat]].
[39] D. D. Dietrich, F. Sannino, Phys. Rev. **D75**, 085018 (2007) [hep-ph/0611341].
[40] R. Gupta, G. W. Kilcup, S. R. Sharpe, Phys. Rev. **D38**, 1278 (1988);
M. Creutz, Phys. Rev. **D38**, 1228-1238 (1988).